AAEC/E146

AAEC/E146

AUSTRALIAN ATOMIC ENERGY COMMISSION

RESEARCH ESTABLISHMENT
LUCAS HEIGHTS

BUCKLING AND INTEGRAL SPECTRUM MEASUREMENTS IN U235 FUELLED SUB-CRITICAL ASSEMBLIES MODERATED BY BeO/FERTILE MATERIAL MIXTURES

by

D.B. McCULLOCH*
P. DUERDEN
E. BRITTLIFF

*Attached from U.K.A.E.A. Reactor Group

December 1965

AUSTRALIAN ATOMIC ENERGY COMMISSION
RESEARCH ESTABLISHMENT
LUCAS HEIGHTS

BUCKLING AND INTEGRAL SPECTRUM MEASUREMENTS IN U235 FUELLED SUBCRITICAL ASSEMBLIES MODERATED BY BeO/FERTILE MATERIAL MIXTURES

by

D. B. McCULLOCH *
P. DUERDEN
E. BRITTLIFF

* Attached, from United Kingdom Atomic Energy Authority

ABSTRACT

Exponential experiments have been carried out to give the materials buckling of a number of near-homogeneous U235/aluminium alloy fuelled systems having fertile oxides intimately mixed with the BeO moderator. Relative fission rates of U235, U233, and Pu239 were also measured in the equilibrium spectrum region of each assembly. Five assemblies having 5 w/o natural uranium oxide in BeO were investigated for a range of BeO/U235 atomic ratios from 1500 : 1 to 5700 : 1. A similar range covering four assemblies was examined for 5 w/o thorium oxide in BeO.

A comparison of the experimental results with diffusion theory calculations is included.

CONTENTS

(continued)

CONTENTS (continued)

1. INTRODUCTION

A series of near–homogeneous subcritical experiments is being carried out using U235, U233, and plutonium fuels diluted with pure BeO, or with BeO/natural uranium or BeO/thoria mixtures.

Buckling and fission rate measurements have already been reported (Duerden et al. 1964) for U235 fuel and beryllia. This report describes similar measurements for systems employing the same U235/aluminium alloy fuel strips and a 5 w/o mixture of natural uranium oxide or thorium oxide in BeO.

2. MATERIALS

The U235/aluminium alloy contained 23.4 w/o of uranium enriched to 89.41 per cent. in the U235 isotope, and was in the form of strips 24 in long by 1.330 in wide by 0.040 in thick. A total of 177 strips was available for these experiments, each containing approximately 14.5 g U235. Full details of the fuel are given in Appendix 1.

The moderator/fertile oxide mixtures were of similar form for both the BeO/$U^{nat.}$ and the BeO/Th lattices. Approximately 5 w/o of the resonance absorber oxide was intimately mixed with the BeO, and the resulting mixture cold pressed and sintered in hydrogen for urania or air for thoria, to form bricks 3 in square by 1 in thick, each weighing about 250 g. Sixty–four bricks were then loaded into a tray, consisting of an aluminium–channel section frame to which was welded a 25 in square by 22 s.w.g. aluminium sheet. The 24 in x 1 in inside faces of the channel section were lined with 0.036 in thick cadmium sheet, and the resulting 24 in square x 1 in thick slab mixture was sealed by an aluminium lid, the outside of which had 12 equispaced parallel slots 1.36 in wide machined to take the U235/Al fuel strips. Thirty trays were filled for each fertile oxide, and to allow access for counters each was pierced by two holes through the 1 in dimension which were lined by aluminium tubes sealed to the top and bottom lids.

Six trays of each composition also were provided with a similar aluminium–lined hole through the 24 in dimension, three of these being parallel, and three perpendicular to the fuel slots. A drawing of a complete canned slab is shown in Figure 2 and full details for the BeO/natural uranium oxide and BeO/thorium oxide are given in Appendices 2 and 3 respectively.

3. EXPERIMENTAL ARRANGEMENTS

The compositions of the nine assemblies studied are given in Table 1. Lattices U I(a) and U I(b) differ only in the geometrical arrangement of the fuel elements. Representative sections of the lattices are shown in Figures 3 to 7. Each assembly consisted of 30 trays of mixture, arrayed with fuel channels running E – W in a horizontal plane (see Figure 8). A general view of a completed stack is shown in Figure 1.

The reactor MOATA (Marks 1962) was used as a neutron source to excite the assemblies, which were built on a 1 in thick by 3 ft square steel plate placed on the reactor top shield, centrally over the open IR 1 stringer hole. A central hole 22 in square was cut in the steel sheet and filled with polythene slabs to help diffuse the neutrons into the graphite plinth, which was 24 in square and 8 in high. The plinth was supported about ¼ in above the steel plate by means of two steel strips 1 in wide and 30 in long under its extreme north and south edges. A 5 in x 1 in steel bar was laid on the protruding ends of these strips at the face of the plinth to carry the east plinth face shielding, so enabling a cadmium sheet to be placed beneath the assembly for 'background flux' measurements without the need for any dismantling. Shielding round the plinth consisted of 0.036 in cadmium sheet and a 4 in thickness of interlocking lead bricks, which reduced the thermal neutron and γ radiations to workable levels.

The BeO/fertile oxide trays, with the necessary fuel strips, were built centrally onto the graphite plinth, the vertical access holes being aligned through each slab by means of 21/64 in diameter silver–steel rods. A cadmium sheet was placed over the top tray, and accidental relative movement of the trays was prevented by means of a light aluminium angle clamping frame held in position by threaded ⅜ in diameter steel tie–rods. The stack dimensions are included in Table 11.

A polythene tent on a light Dexion frame, and fitted with filtered air extract equipment, effectively checked any spread of beryllium contamination. No significant quantities of neutron reflecting materials were present within 20ft of the sides and top of the stacks.

4. MEASUREMENT OF THE MATERIALS BUCKLING

Horizontal and vertical flux distributions in the stacks were measured using ¼ in diameter BF_3 proportional counters. All counts were taken with reference to a preset number of pulses from a 1 in diameter U235 fission counter (containing 135 mg U235) fixed firmly in the reactor shield–tank water at a position giving 800,000 pulses a minute at a reactor power of 5 kW. Flux scanning was thus rendered independent of drift in reactor power level.

Routine noise and gain checks were made for each counting channel before commencing each day's run. Checks were also made for presence of spurious counts at operating settings, and to ensure that the bias characteristics of the channels had not deteriorated. In addition, the counter was returned to a fixed 'monitor' position in the stack at frequent intervals to provide an overall check on freedom from drift during the course of a scan. The aim was to achieve an overall accuracy of ± ½ per cent. or better on the flux measurement at any position.

4.1 Extrapolated Widths

Horizontal scans were made at three different heights in each stack in both x and y directions. Measurements were also made with the counter covered by cadmium to ensure that only measurements made in the region of equilibrium spectrum were included in the subsequent analysis.

4.1.1 Errors

The following sources of error were considered for horizontal flux scans.

(a) Statistical Error

60,000 counts or more were taken at each measuring position, contributing ± 0.41 per cent.

(b) Control Channel Statistics

Not less than 800,000 control counts were required to collect 60,000 counts in the stack. The resulting error was therefore always < ± 0.11 per cent.

(c) Counter Positioning

The location accuracy was better than ±1/64 in. At the extreme outer measuring points of the horizontal distributions, this corresponds to the maximum flux uncertainty of 0.27 per cent. The counter is always positioned at least twice for each flux measurement, giving an error always < ± 0.19 per cent.

(d) Paralysis Time

This was measured as 3.5 ± 0.5 μs. The maximum correction was < 0.6 per cent. and, within any scan, the relative correction did not exceed 0.3 per cent. The resulting error is therefore < ± 0.05 per cent.

(e) Drifts of Counter Sensitivity

Substitution of the 1 in fission counter for the 1 in BF_3 counter used by Duerden et al. (1964) reduced the inter–channel drift to ± 0.25 per cent. For two positionings of the counter, this contributes ± 0.18 per cent

Combination of the above sources of error gives a total error of ± 0.5 per cent. for fluxes in horizontal scans.

4.2 Relaxation Lengths

Vertical scans were made in two positions, one with x,y co-ordinates 2 in, 2 in, and the other with co-ordinates -4 in, -4 in, referred to the stack centre. Cadmium ratio measurements were again made as for the horizontal scans.

To ensure that the vertical flux distribution used to obtain the relaxation length for the assembly was solely that due to the required source of neutrons below the stack, it was necessary to subtract any background due to, for example, γ-n neutrons produced by direct γ-radiation from the MOATA core. This was achieved in the natural uranium assemblies by sliding a sheet of 0.036 in cadmium underneath the plinth and repeating the vertical distribution measurements. In the thorium assemblies, the gap between plinth and steel base-plate was slightly increased, and a ¼ in thick boral sheet was substituted for the cadmium. This increased the bare/background ratio and considerably relaxed the accuracy necessary for the background flux measurements, with a consequent substantial saving of time.

4.2.1 Errors

The aim for these experiments was that final flux values from which relaxation lengths were to be derived should be accurate to about ± 0.5 per cent. The attenuation of the cadmium sheet used for the background measurements was about 3.7 for all lattices. Since

$$\sigma^2 = \frac{1}{(f-1)^2} \{(f \times \sigma_T)^2 + \sigma_B^2\} \quad ,$$

where

σ is the fractional error of the final flux value,

σ_T " " " " " " bare flux

σ_B " " " " " " background flux, and

f is the ratio of the bare to background flux,

considerable effort was required to reduce the statistical and positioning uncertainties to the sufficiently low levels required for the final accuracy. In practice this was not quite achieved, the error on the final fluxes being rather better than ± 0.6 per cent., which was considered satisfactory. The method adopted was to take sufficient counts in four scans for the bare measurement to give an overall accuracy for the bare flux of ±0.38 per cent. Sufficient background counts were then taken in either four or two scans as appropriate to give a final error of < 0.6 per cent. in the background-corrected flux.

The errors considered were as follows:

	Bare	Background
(a) Counting Statistics		
Bare - not less than 120,000	± 0.29 per cent.	
Background - from 60000 down to 15000 per position as f ranges from 3.7 to 4.4		± 0.41 per cent. - ± 0.82 per cent.
(b) Control Channel Statistics		
Bare - not less than 1.2×10^6	±0.09 per cent.	
Background - from 10^7 to 10^6		±0.03 per cent. - ±0.1 per cent.

(c) Counter Positioning

	Bare	Background
This was accurate to better than ± 1/64 in. For the worst case of the shortest relaxation length this corresponds to ± 0.35 per cent. in flux.		
Bare – 4 positionings	±0.17 per cent.	
Background – 4 positionings or 2 positionings		±0.17 per cent. – ±0.25 per cent.

(d) Paralysis Time, τ

τ was measured as 3.5 ± 0.5 μs. The maximum paralysis time correction was

Bare < 0.6 per cent.	±0.08 per cent.	
Background < 0.15 per cent.		±0.02 per cent.

(e) Drifts in Counter Sensitivity

The inter–channel drift is ±0.25 per cent. The resulting error contributions are

Bare – 4 positionings	±0.13 per cent.	
Background – 4 positionings or 2 positionings		±0.13 per cent. – ±0.18 per cent.

1036
40

Combination of the above sources of error gives an overall error for the bare count of ±0.38 per cent. The error of the background count ranged from 0.47 per cent. to 0.88 per cent. as f ranged from 3.7 to 4.4. The resulting error in the background–corrected flux was in all cases ±0.56 per cent.

4.3 Results

The measured flux distributions for each lattice are given in Appendices 4 to 9. The errors may in all cases be taken as ±0.5 per cent. for horizontal scan fluxes and ±0.6 per cent. for vertical scan fluxes. Positional co–ordinates x,y are given in terms of distance from the east and north extreme faces of the actual BeO/fertile bricks. z co–ordinates are measured from the top of the graphite plinth.

4.3.1 E – W widths

The flux measurements were made to within 4 in of the stack edges. This region was confirmed to be one of constant cadmium ratio by the cadmium–covered BF_3–counter scans carried out in each lattice (Section 4.3.4) (Appendices 10,11). Scans were made at three different levels in each assembly, one on the y direction centre–line and the other 6 in to the right or left of that line. It was confirmed that these all lay in the region of constant cadmium ratio for each lattice.

The measured flux distributions were each fitted by weighted least–squares to the function:

$$\phi = A \cos \frac{\pi}{a_x} (x - \bar{x}) \quad ,$$

where

ϕ is the flux,

A is an arbitrary constant,

a_x is the extrapolated E – W width of the assembly, and

$\bar{x}$ is the 'centre' of the cosine distribution.

This procedure was carried out for the complete measuring range x = 4in to x = 20 in, and also for x = 5 in to x = 19 in and x = 6 in to x = 18 in. The results are summarised in Tables 2 and 3 for the BeO/UO_2 and BeO/ThO_2 lattices respectively.

Examination of these tables for trends in the data showed:

(i) There is no significant change of the extrapolated widths as the outermost points are omitted from the distribution, the ratios (assuming the statistical errors of the fits to apply) being

$$\frac{a_x\,(x = 5\text{in to } 19\text{in})}{a_x\,(x = 4\text{in to } 20\text{in})} = 1.0005 \pm 0.009, \quad \frac{a_x\,(x = 6\text{in to } 18\text{in})}{a_x\,(x = 5\text{in to } 19\text{in})} = 0.9995 \pm 0.0014 \ .$$

The breakdown for each z–level of measurement (top, middle, bottom) is given in Table 4 and also shows no indication of trend. We conclude that there is no significant perturbation of the cosine distribution by a 'cosh' component due to inleakage of neutrons through the stack sides, or by spectrum changes near the stack boundaries. We cannot however deduce freedom from higher (third) harmonic components, since the outer antinodes of that harmonic lie almost exactly at x = 5 in and x = 19in, so that little variation in fitted width with range would be caused by a reasonably sized third harmonic component for the particular ranges used in these experiments.

(ii) There is no significant asymmetry in the distribution, when allowance is made for relative displacements of ±1 mm which may be present at any particular scanning level owing to variations from tray to tray of the distance between the edge of the BeO/fertile mixture and the edge of the aluminium lids of the scanning and adjacent trays, against which the locating boss of the counter is positioned for reference.

(iii) There is no significant systematic trend of the extrapolated width from lattice to lattice, although the scatter of individual measurements for a given z is greater than would be expected from the statistical errors of the cosine fits.

(iv) There is a marked variation of extrapolated width with the height in the stack at which it was measured, the overall ratio for top/bottom being 1.014 ± 0.002 .

Only small differences in spectrum, as indicated by boron cadmium ratio measurements, were observed between the lowest and highest horizontal scanning holes, and since no dependence of the extrapolated width on lattice composition was observed, it is unlikely that spectrum changes could account for the observed trend.

It is possible that a third harmonic component might be present in the distribution, of adequate amplitude to account for the effect, although evidence in support of this is not easily discernible from the comparison of corner and centre hole relaxation lengths in each lattice. However, in view of the large central peak in the neutron source due to the small area of the IR1 stringer hole a positive third harmonic component is by no means unlikely, and the 4→20 range flux distributions were therefore least–squares fitted to the function:

$$\phi = A \cos \frac{\pi(x - \bar{x})}{a_x} + B \cos \frac{3\pi(x - \bar{x})}{a_x} \ .$$

The results are given in Tables 5 and 6.

The error of an individual value of a_x has now risen to about ±0.8 cm, and all the values in the table are self–consistent. The mean values for each level are also self–consistent, and lead to an overall mean of 65.82 ± 0.15 cm, which is very close to the mean value for the fundamental only fits to the same data (65.86 cm), which did not however constitute a self–consistent set.

Unfortunately, whilst the harmonic fits to the lowest level data in all cases but one yield positive values of B/A as anticipated, the middle and top levels give predominantly negative values, suggesting that the third harmonic component may not be the complete, even if the substantially correct, explanation. In the absence of an alternative explanation for the trend of extrapolation width with height of measurement, we therefore adopt the mean value of 65.82 cm, but with an increased error of ± 0.37 cm which covers the possibility that either the top or bottom position mean values from the fundamental fits could be representative of the true extrapolated E – W width of the stack.

4.3.2 N – S widths

Flux scans were again made at three different levels of each stack to within 4 in of the stack boundaries, embracing a region shown to have constant boron cadmium ratio. For N – S scans however, which ran perpendicular to the direction of the long dimension of the fuel elements, neutron flux fine structure effects were present. The method used for treatment of the N – S flux scans has been reported by Brittliff and Duerden (1965).

Fine structure calculations have been carried out based on a one-dimensional slab cell calculation. The appropriate one-dimensional cells of each lattice are shown in Appendix 12. Correction factors were calculated and were applied to the measured fluxes. The measured fluxes and the corrected fluxes are tabulated in Appendices 6 and 9. The correction factors used are shown in Appendix 13. The maximum correction factor applied was 5 ± 0.5 per cent.; the overall error in the corrected flux was therefore ± 0.7 per cent.

The corrected flux distributions were each fitted by weighted least squares to the function:

$$\phi = A \cos \frac{\pi (y - \bar{y})}{a_y} ,$$

where ϕ is the corrected flux,

A is an arbitrary constant,

a_y is the extrapolated N – S width of the assembly, and

$\bar{y}$ is the 'centre' of the cosine distribution.

This procedure was carried out for the complete measuring range x = 4 in to x = 20 in and also for the range x = 5 in to x = 19 in. The results are summarised in Tables 7 and 8 for the BeO/UO_2 and BeO/ThO_2 lattices respectively.

Examination of these tables for trends in the data resulted in similar conclusions to those obtained from examination of the E – W widths.

(i) There is no significant change of the extrapolation width as the outermost points are omitted from the distribution:

$$\frac{a_y (y = 5 \text{ in to } 19 \text{ in})}{a_y (y = 4 \text{ in to } 20 \text{ in})} = 1.0004 \pm 0.0018 .$$

(ii) The breakdown for each z level of measurement (top, middle, bottom) is given in Table 9. There is no systematic trend of extrapolated width from lattice to lattice.

(iii) There is a marked variation of the extrapolated width with the height in the stack at which it was measured, the overall ratio for top/bottom being 1.007 ± 0.004. It is possible that a third harmonic component may be present in the distribution but this could not be checked as an insufficient number of flux measurements were made in the N – S scans. We have adopted the mean value of 66.53 cm, but with an increased error of ± 0.18 cm which covers the possibility that either the top or bottom position mean values could be representative of the true extrapolated N – S width of the stack.

4.3.3 Relaxation lengths

It was necessary to ensure that only measurements from the region of constant boron cadmium ratio were included in the analysis of vertical flux distributions. This immediately restricted the range of measurement to 41 cm < z < 72 cm, and even then it was necessary in lattices U III, U IV, and Th III, Th IV to load the lowest tray more heavily with fuel than the remainder of the stack to produce this region of equilibrium spectrum. In fact, subsequent detailed inspection of the cadmium ratio measurements from all the lattices showed a tendency for the ratios at z = 41 cm and z = 72 cm to differ systematically from the remainder, so these positions were excluded from the analysis.

The remaining fluxes were least–squares fitted to the function:

$$\phi = A \sinh \frac{h - z}{b_{II}} \quad ,$$

where h is the extrapolated height of the stack,

b_{II} is the relaxation length of the fundamental mode flux, and

A is a constant.

The fitted values of b_{II} and h for centre and corner holes of each lattice are given in Table 10, which also shows the effect on h and b_{II} as points from the bottom of the measuring range, that is z = 43 cm and z = 47 cm, are successively omitted from the analysis.

Examination of Table 10 shows that for the widest range analysis, there is a systematic difference between centre and corner hole b_{II} values, the centre hole having the smaller value. Whilst the difference is only of comparable size to the experimental error, the systematic trend is disturbing and does support the hypothesis of a third harmonic component as suggested by the E – W horizontal scans.

When the data at z = 43 cm are omitted, the systematic difference disappeared, and the centre hole/corner hole differences are compatible with the errors of the fits. There is no significant improvement on further omission of the data for z = 47 cm, and we therefore conclude that the range 47 cm < z < 69 cm is adequately free from harmonic effects within the experimental errors. The final mean value of relaxation length for each lattice is given in Table 10.

4.3.4 Cadmium ratio measurements

Boron cadmium ratio traverses were made along x, y, and z directions of each stack, and confirmed that within the experimental accuracy (approximately ± 2 per cent.), the ratio was in all cases constant over the measuring range included in the analysis of the experiments (see Appendix10).

4.3.5 Extrapolated lengths

The mean extrapolated heights together with the mean horizontal extrapolated lengths are given in Table 11.

4.3.6 The materials buckling

The bucklings and the components used in their calculation are quoted in Table 12.

Because of the heterogeneous nature of the stacks, we have:

$$K^2 = \frac{M_{II}^2}{M^2}\left\{\left(\frac{\pi}{a_x}\right)^2 + \left(\frac{\pi}{a_y}\right)^2\right\} - \frac{M_1^2}{M^2}\left(\frac{1}{b_{II}}\right)^2 \quad ,$$

where

K^2 is the materials buckling of an homogeneous lattice of the same composition as the experimental stack (neglecting the effects of fine structure),

M^2 is the migration area in the corresponding homogeneous lattice, and

$M_{\parallel}^2$, $M_{\perp}^2$ are the migration areas for the experimental lattice, respectively parallel and perpendicular to the slabs.

Keane (1965) has suggested a method of estimating $M_{\parallel}^2/M_{\perp}^2$ for the case of a small gap of a strongly absorbing medium between layers of moderator, and we assume without significant error that $M_{\perp}^2 = M^2$. Keane's method gives $M_{\parallel}^2/M_{\perp}^2 = 1.006$ for Lattice I, 1.018 for Lattice II, 1.028 for Lattice III and 1.034 for Lattice IV.

It can be seen from Table 12 that the values of materials buckling obtained by putting $M_{\parallel}^2/M_{\perp}^2 = 1$ are considerably different from the values obtained by using the asymmetry correction factors obtained by Keane's method.

It is reasonable to assume that the corrected value of the materials buckling will be closer to the true value though a large uncertainty is to be expected. A more definite conclusion would be obtained by using a more rigorous theoretical treatment of the anisotropy.

5. INTEGRAL SPECTRUM MEASUREMENTS

The relative fission rates of U235, U233, and Pu239 were measured, using fission chambers intercalibrated in a thermal neutron flux as described by Duerden et al. (1964). However the use of ¼ in diameter fission chambers with integral rigid stems, together with some modifications in technique, enabled improved accuracy to be obtained. The important features of the fission chambers are shown schematically in Figure 9A.

5.1 Lattice Measurements

Each chamber was radiographed to determine the position of its active volume. The distance from the reference face of the connector boss to the centre of the active volume was the same for all available chambers to within 0.01 in. An insulated spacer tube (Figure 9B) was used to position the centre of the active volume exactly at the centre of the lattice with the counter installed in a horizontal flux scanning hole. The connector boss of the counter was always supported to ensure that the active tip lay on the bottom of the flux scanning hole.

Thermal flux calibration measurements were performed immediately before and immediately after each lattice relative reaction rate measurement, which was carried out twice.

5.2 Thermal Column Measurements

The arrangements were similar to those described by Duerden et al. (1964) except that the aluminium access tube was replaced by a Perspex tube fitted with an internal collar against which the reference face of each fission chamber rested to ensure correct vertical location of the active volume.

The lowest 15 inches of the access tube was of reduced diameter to pass through the aluminium "flux-flattening" box and was further reduced in internal diameter by a polythene liner such that radial clearance round the active volume was only 1/64 in approximately.

5.3 Flux Depression due to Fission Chamber Wall Material

The fissile material in each chamber was coated on the inner surface of a 0.005 in thick cylinder of stainless steel which was in turn surrounded by a nickel cylinder of 0.020 in wall thickness (see Figure 9A). The effect of these materials on the reaction rate of each fissile material will in general be different in the lattice spectrum and in the thermal column, and will give rise to systematic errors in the relative fission rate measurements if not corrected for.

Nickel sleeves 2 in long by 0.25 in internal diameter, of wall thickness 0.010 in, 0.020 in, and 0.030 in, were available. The count rate of each chamber was measured in all the U235/U238 BeO lattices bare and with each nickel sleeve in turn placed over the active length of the chamber.

Extrapolation of the data to zero nickel thickness by least squares fit to a straight line enabled the effect of the chamber wall to be determined. Similar measurements were also made in the near-thermal flux at the base of the graphite plinth below the stack.

For each chamber the flux depression due to the nickel wall was plotted as a function of spectrum hardness, as indicated by the boron cadmium ratio. The results (shown in Figure 10) were an excellent fit to a linear relation, and the least squares fitted parameters were used to obtain the depression factor for each chamber in the thermal column flux, and the depression ratio for each lattice relative to that in the thermal column.

Stainless steel sleeves of 0.015 in and 0.030 in were also available, but measurements in the thermal column and in the hardest 'spectrum' lattice showed the depression due to the 0.005 in stainless steel of the chamber to be very small and identical, within errors, in the thermal column and the lattice (see Figure 11). Thus no further measurements were made.

5.4 Errors

Following Duerden et al. (1964), random and systematic sources of error contributing to the uncertainty of the final fission ratios for each lattice are considered separately. The magnitude of each source of error is given as its contribution to the measured ratio.

5.4.1 Random errors--thermal calibrations

(a) Statistical or Counting Error

Approximately 100,000 counts were taken with each chamber, giving a contribution to the error on each ratio of 0.46 per cent.

(b) Control Channel Statistics

At least 500,000 control counts were needed whilst accumulating 100,000 counts from the chambers, resulting in a maximum error contribution of 0.2 per cent.

(c) Count Channel Gain Drifts

Analysis of the count channel discriminator bias settings as determined by the stable amplitude pulse generator showed the mean change over the course of one thermal calibration plus one lattice measurement to be 0.55 volts. Day-to-day changes were of similar size and there is no reason to assume that over twenty minutes or so of a thermal calibration the drift is any less; the discrimination setting for the U233 or Pu239 chamber may differ by ± 0.25 volts, relative to the U235 chamber. This corresponds to an uncertainty in either ratio of 0.5 per cent.

(d) Control Channel Sensitivity Drift

Analysis of measurements made of drift between the control and another similar channel suggest the error in count ratio due to this source is 0.2 per cent.

(e) Counter Positioning

Both axial and radial positioning were accurate to better than 1/64 in and the resulting uncertainty is 0.1 per cent.

(f) Paralysis Time

The paralysis time was measured as 2.5 ± 0.5 μs. The maximum correction applied was 1.5 per cent., giving a maximum error contribution of 0.3 per cent.

(g) Total Random Error

Combination of the above random sources of error gives the uncertainty of a single measurement of the U233/U235 and Pu239/U235 ratios in the thermal flux as ± 0.8 per cent.

5.4.2 Random errors–lattice measurements

The error contributions are identical to those for the thermal calibration measurements except for:

(a) Statistics

40,000 counts were obtained with each chamber giving a resulting uncertainty in the ratio of 0.7 per cent.

(b) Control Statistics

At least 10^6 counts were needed. The resulting error contribution is < 0.1 per cent.

(c) Counter Positioning

Uncertainty in horizontal and vertical direction was about 0.01 in. The consequent uncertainty in the ratio due to the horizontal positioning is negligible and that due to the vertical positioning is ~ 0.2 per cent.

(d) Paralysis Time

U233 and Pu239 count rates were obtained using the DIRECT setting of the scaler, the measured dead time for which is 196 ± 20 μs. The maximum correction applied was 0.5 per cent., the resulting error being 0.05 per cent.

The U235 count rate was obtained through a fast decade with a dead time of 2.5 μs. The resulting error is negligible.

(e) Total Random Error

Combining the above sources of error gives the uncertainty on a single ratio measurement in the lattices of ± 0.9 per cent.

5.4.3 Systematic errors

(a) Chamber Wall Depressions

The mean of the thermal calibration ratios comprising a set, was corrected for nickel wall flux depression using the intercept of the straight line fits shown in Figure 10. Since the stainless steel correction was identical, no correction has been applied, but an uncertainty corresponding to the experimental error of this determination has been allowed for. The mean thermal calibration data quoted in the results tables have errors including the uncertainty in the wall correction which in all cases is 0.58 per cent for nickel and 0.14 per cent for the stainless steel, making a total of 0.6 per cent.

The lattice count ratios are corrected for wall depressions using figure 10 and the measured boron cadmium ratios. The uncertainty in the correction is determined by the uncertainty in the slopes, and its contribution to the uncertainty in the measured ratio is from 0.9 per cent. for the hardest to 0.35 per cent. for the softest spectrum. The stainless steel uncertainty contributes ±0.25 per cent.

(b) Position of Active Volume

There is an uncertainty of approximately ± 0.010 inch in the position of the centres of the active volumes of the chambers. Since the thermal calibrations were carried out in an effectively uniform flux whilst the gradient in the lattices was of the order of 2 per cent. per inch this uncertainty contributes possible systematic errors to the fission ratios per fissile atom of a maximum of 0.1 per cent.

(c) Fission Cross Section Data

Data for the Maxwellian fission cross sections used in conjunction with the thermal column measurements to calculate the fission ratios per fissile atom were taken from Westcott (1960) and the relative accuracy is approximately ± 1.0 per cent.

5.4.4 Total error

When all the above sources of error are considered the error in the fission ratio per fissile atom for any lattice lies within the range 1.75 to 1.63 per cent.

5.5 Results

The fission ratios per fissile atom are given in Table 13 whilst the relative count rates as measured in the lattices and the thermal column are given in Appendices 14 and 15.

6. COMPARISON OF EXPERIMENTS WITH THEORY

Critical size calculations were carried out for bare homogeneous spherical reactor systems with the compositions used in the assemblies. The multigroup diffusion theory code, CRAM (Hassitt 1962) was used, with an 18-group cross section library. The cross sections are basically those listed by Bell (1963) but were modified as follows:

BeO Upscattering has been included based upon data generated by PIXSE (McDougal 1963) using a tabulation of $S(\alpha, \beta)$ (Sinclair 1962) obtained from LEAP (McLatchie 1962). This has been included by reducing the self-scattering term and maintaining σ_{tr} as the value given by Bell.

U235 The value of $\overline{\nu}$ used is that due to Smith (1964). Self-shielding factors were calculated on the basis of the U235 and aluminium being intimately mixed in a fuel plate and using tables published by Argonne National Laboratory (1963). A value of σ_p = 100 barns was used.

U238 For the thoria lattices the self-shielding factors were calculated for U238 mixed with aluminium in a fuel plate. σ_p = 400 barns, and again tables published by Argonne National Laboratory (1963) were used.

For the urania lattices self-shielding factors were calculated on the basis of urania and beryllia being intimately mixed in a moderator tray; σ_p = 2000 barns.

Th232 The cross sections used were obtained from the LASL 16-group set listed by Roach (1960), by extending them to 18 groups. Groups 1 – 15 cross sections are the same; cross sections for groups 16, 17, and 18 were derived from the graphical compendium of Hughes (1958). The group boundaries between groups 6 and 15 of our set and the Roach set are slightly different. The self-shielding factors were calculated for a moderator tray, using the resonance parameters listed by Garg et al. (1964) (σ_p = 2000 barns).

The cross sections used are listed in Appendix 16. Normalised neutron fluxes at the centre of the critical spheres are shown in Figures 12 and 13.

The materials bucklings of the assemblies were calculated using the critical radii and the experimental value of the extrapolation distance, and are shown in Figures 14 and 15. For the urania assemblies it can be seen that the calculated values of materials buckling are similar to

the experimental values obtained using Keane's method for calculation of $M_{\parallel}^2/M_{\perp}^2$. The calculated materials buckling for the thoria assemblies are much smaller than the experimental values.

Fission ratios have been calculated using the spectra at the centre of the critical spheres, listed in Appendix 17. The fissile material in the detectors was assumed to be infinitely dilute. It can be seen from Figures 16 and 17 that the calculated Pu239/U235 ratios are approximately 25 per cent. higher than the experimental values; the calculated U233/U235 ratios are approximately 10 per cent. higher than the experimental values. The experimental and calculated results are compared in Table 14.

Similar calculations have been carried out on BeO/U235 mixtures. The material compositions used are those reported by Duerden et al. (1964). It can been seen from Figure 18 and 19 that the agreement between experimental and calculated materials buckling for these assemblies is similar to that obtained for the BeO/UO_2/U235 assemblies. The experimental results reported by Duerden et al. (1964) are compared with these calculations in Table 15.

The treatment of the thoria appears therefore to be the main source of error in the BeO/ThO_2/U235 assembly calculations. The calculated Pu239/U235 ratios for the BeO/U235 assemblies are approximately 20 per cent. higher than the experimental values; the calculated U233/U235 ratios are approximately 5 per cent. higher than the experimental values.

7. CONCLUSIONS

The materials bucklings of the assemblies have been calculated from measurements of the relaxation length and the extrapolation width for the assemblies; an accuracy of 5 to 20 per cent. was achieved. A correction for anisotropy has to be included however and the application of this correction, which is only of the order of 2 per cent., can change the calculated materials buckling by between 2 and 40 per cent. Relative fission ratios have been measured to approximately ± 2 per cent.

Some simple calculations have been carried out. Good agreement was obtained for the materials buckling of the urania lattices but the calculated materials buckling of the thoria lattices was too small.

The calculated Pu239/U235 ratios were approximately 25 per cent. higher than the experimental values and the calculated U233/U235 ratios were approximately 10 per cent. higher than the experimental values.

Calculations are in progress to resolve these differences.

8. ACKNOWLEDGEMENTS

We wish to thank the MOATA operation team for counting and general assistance in the experimental work.

9. REFERENCES

Argonne National Laboratory (1963). – ANL5800.

Bell, G.I., et al. (1963). – LAMS 2941.

Brittliff, E., and Duerden, P. (1965). – AAEC/E 145.

Duerden, P., McCulloch, D.B., and Brittliff, E. (1964). – AAEC/E 123.

Garg, J.B., Petersen, J.S., and Havens, W.W. (1964). – Phys. Rev. 134 (5B):985.

Hassitt, A. (1962). – TRG 229 (R).

Hughes, D.J. and Schwartz, R.B. (1958). – BNL 325.

Keane, A. (1965). – AAEC/TM

Marks, A.P. (1962). – Atomic Energy 5 (4): 9–21.

McDougal, J.D. (1963). – AEEW – M – 318.

McLatchie, R.E.C. (1962). – UKAEA Internal Report.

Roach, W.H. (1960). – Nucl. Sci. & Engng. 8 (6): 621.

Smith, A.B. (1964). – ANL 6792.

Sinclair, R.N. (1962). – AERE NP. GEN 28.

Westcott, C.H. (1960).– AECL 1101.

TABLE 1

LATTICE COMPOSITIONS

Composition of Homogeneously Smeared Experimental Lattices in Atoms per cm^3

Element	U I (a and b)	U II	U III	U IV
Be	3.436×10^{22}	3.436×10^{22}	3.436×10^{22}	3.436×10^{22}
O	3.8×10^{20}	3.6×10^{20}	3.5×10^{20}	3.4×10^{20}
~~O~~	~~3.474×10^{22}~~	~~3.472×10^{22}~~	~~3.471×10^{22}~~	~~3.470×10^{22}~~
Al	4.389×10^{21}	4.164×10^{21}	3.931×10^{21}	3.855×10^{21}
~~U234~~	~~2.558×10^{17}~~	~~1.761×10^{17}~~	~~9.638×10^{16}~~	~~6.980×10^{16}~~
U235	2.255×10^{19}	1.542×10^{19}	8.290×10^{18}	5.914×10^{18}
~~U236~~	~~7.845×10^{17}~~	~~5.230×10^{17}~~	~~2.615×10^{17}~~	~~1.744×10^{17}~~
~~U238~~	~~1.644×10^{20}~~	~~1.639×10^{20}~~	~~1.634×10^{20}~~	~~1.633×10^{20}~~
U8	1.654×10^{20}	1.646×10^{20}	1.638×10^{20}	1.635×10^{20}

Element	Th I a	Th II	Th III	Th IV
Be	3.474×10^{22}	3.474×10^{22}	3.474×10^{22}	3.474×10^{22}
O	3.9×10^{20}	3.7×10^{20}	3.6×10^{20}	3.5×10^{20}
~~O~~	~~3.513×10^{22}~~	~~3.511×10^{22}~~	~~3.510×10^{22}~~	~~3.509×10^{22}~~
Al	4.407×10^{21}	4.179×10^{21}	3.950×10^{21}	3.874×10^{21}
Th232	1.703×10^{20}	1.703×10^{20}	1.703×10^{20}	1.703×10^{20}
~~U234~~	~~2.395×10^{17}~~	~~1.597×10^{17}~~	~~7.983×10^{16}~~	~~5.322×10^{16}~~
U235	2.139×10^{19}	1.426×10^{19}	7.128×10^{18}	4.752×10^{18}
~~U236~~	~~7.848×10^{17}~~	~~5.232×10^{17}~~	~~2.616×10^{17}~~	1.744×10^{17}
~~U238~~	1.510×10^{18}	1.007×10^{18}	5.032×10^{17}	3.355×10^{17}
U8	2.535×10^{18}	1.690×10^{18}	8.446×10^{17}	5.631×10^{17}

Be O
(A)
Al
U5
U8
Th

TABLE 2

EXTRAPOLATED x – WIDTHS FOR BeO/UO_2 ASSEMBLIES

Lattice	Position		10.16 cm < x < 50.80 cm		12.70 cm < x < 48.26 cm		15.24 cm < x < 45.72 cm	
	z = (cm)	y = (cm)	a_x (cm)	$\Sigma \frac{\delta^2}{\sigma^2}$ (For 17 Points)	a_x (cm)	$\Sigma \frac{\delta^2}{\sigma^2}$ (For 15 Points)	a_x (cm)	$\Sigma \frac{\delta^2}{\sigma^2}$ (For 13 Points)
U Ia	39.19	15.24	64.96 ± 0.16	10.2	64.93 ± 0.26	10.2	64.27 ± 0.39	4.8
	50.38	30.48	65.91 ± 0.16	9.5	66.09 ± 0.26	8.6	66.36 ± 0.41	7.4
	67.18	45.72	65.61 ± 0.16	10.6	65.21 ± 0.26	6.4	65.23 ± 0.40	5.4
U Ib	44.79	15.24	65.15 ± 0.16	18.9	64.88 ± 0.24	16.9	64.84 ± 0.38	16.9
	50.38	30.48	65.81 ± 0.17	10.9	66.17 ± 0.26	6.1	66.06 ± 0.40	5.0
	67.18	45.72	66.13 ± 0.17	15.9	66.54 ± 0.26	8.4	66.10 ± 0.40	5.0
U II	44.79	15.24	65.37 ± 0.16	14.8	65.07 ± 0.23	11.7	64.99 ± 0.33	7.6
	50.38	30.48	65.80 ± 0.17	7.6	66.08 ± 0.25	5.6	65.92 ± 0.38	5.2
	67.18	45.72	66.33 ± 0.17	18.9	66.03 ± 0.26	16.5	66.84 ± 0.41	5.8
	67.18	45.72	66.64 ± 0.17	18.9	66.61 ± 0.26	18.9	67.23 ± 0.41	14.6
U III	44.79	15.24	65.51 ± 0.17	6.3	65.51 ± 0.26	6.3	65.36 ± 0.41	6.0
	50.38	30.48	65.48 ± 0.16	6.4	65.53 ± 0.25	6.3	65.30 ± 0.39	5.7
	67.18	45.72	66.34 ± 0.16	8.5	66.60 ± 0.25	5.5	66.74 ± 0.39	5.5
U IV	44.79	15.24	65.39 ± 0.16	12.4	65.33 ± 0.26	10.5	65.14 ± 6.38	10.0
	50.38	30.48	65.94 ± 0.17	8.7	66.20 ± 0.26	6.9	65.99 ± 0.40	6.4
	67.18	45.72	66.32 ± 0.17	16.8	66.72 ± 0.25	7.2	66.67 ± 0.41	6.4

TABLE 3

EXTRAPOLATED x – WIDTHS FOR BeO/ThO_2 ASSEMBLIES

Lattice	Positions		10.16 cm < x < 50.80 cm		12.70 cm < x < 48.26 cm		15.24 cm < x < 45.72 cm	
	z =(cm)	y =(cm)	a_x (cm)	$\Sigma \frac{\delta^2}{\sigma^2}$ (For 17 Points)	a_x (cm)	$\Sigma \frac{\delta^2}{\sigma^2}$ (For 15 Points)	a_x(cm)	$\Sigma \frac{\delta^2}{\sigma^2}$ (For 13 Points)
Th Ia	50.38	30.48	65.99 ± 0.17	5.3	65.77 ± 0.25	4.1	65.88 ± 0.39	3.8
	58.78	15.24	65.86 ± 0.17	8.7	65.62 ± 0.25	6.9	65.93 ± 0.39	4.5
	58.78	15.24	65.76 ± 0.16	8.0	65.60 ± 0.25	6.8	65.96 ± 0.39	4.8
Th II	50.38	30.48	65.79 ± 0.17	5.0	65.78 ± 0.25	4.5	65.70 ± 0.39	4.2
	58.78	15.24	65.69 ± 0.16	9.8	65.68 ± 0.25	9.6	65.60 ± 0.39	8.8
	67.18	45.72	66.20 ± 0.17	7.9	66.23 ± 0.26	7.0	66.02 ± 0.40	1.8
Th III	50.38	30.48	65.52 ± 0.16	14.7	65.49 ± 0.25	14.7	65.88 ± 0.39	8.4
	58.78	15.24	65.69 ± 0.16	9.9	65.57 ± 0.25	8.4	65.92 ± 0.39	7.2
	67.18	45.72	66.54 ± 0.17	9.6	66.62 ± 0.26	9.3	67.14 ± 0.41	5.3
Th IV	50.38	30.48	65.83 ± 0.17	11.9	66.10 ± 0.26	10.0	65.84 ± 0.39	9.4
	58.78	15.24	65.86 ± 0.17	6.9	65.86 ± 0.25	5.0	65.64 ± 0.39	4.2
	67.18	45.72	66.48 ± 0.17	14.7	66.27 ± 0.26	12.7	66.43 ± 0.40	12.0

TABLE 4

VARIATION OF MEAN E – W WIDTHS (cm) WITH HEIGHT

Position	Lattice				
	U Ia	U Ib	U II	U III	U IV
Bottom	64.72 ± 0.16	64.96 ± 0.16	65.14 ± 0.16	65.46 ± 0.16	65.29 ± 0.16
Middle	66.12 ± 0.16	66.01 ± 0.16	65.93 ± 0.16	65.44 ± 0.16	66.04 ± 0.16
Top	65.35 ± 0.16	66.26 ± 0.16	66.61 ± 0.16	66.56 ± 0.16	66.57 ± 0.16

Position	Lattice			
	Th Ia	Th II	Th III	Th IV
Bottom	65.88 ± 0.16	65.76 ± 0.16	65.63 ± 0.16	65.92 ± 0.16
Middle	65.80 ± 0.16	65.66 ± 0.16	65.73 ± 0.16	65.79 ± 0.16
Top	65.77 ± 0.16	66.15 ± 0.16	66.77 ± 0.16	66.39 ± 0.16

Mean Bottom Width	65.42 ± 0.05 cm
Mean Middle Width	65.84 ± 0.05 cm
Mean Top Width	66.32 ± 0.05 cm

TABLE 5

EXTRAPOLATED x–WIDTHS FOR 3RD HARMONIC FITS OF BeO/UO_2 ASSEMBLIES

Lattice	Position		10.16 cm < x < 50.80 cm				
	z = (cm)	y = (cm)	a_x (cm)	λ_x (cm)	A	B	$\Sigma \frac{\delta^2}{\sigma^2}$
U Ia	39.19	15.24	66.07 ± 0.66	2.56 ± 0.33	6966 ± 30	61.5 ± 37.0	8.3
	50.38	30.48	64.76 ± 0.54	1.90 ± 0.27	4642 ± 16	−41.9 ± 20.0	7.1
	67.18	45.72	66.72 ± 0.70	2.88 ± 0.35	1244 ± 5.6	10.6 ± 6.9	8.9
U Ib	44.79	15.24	66.73 ± 0.90	2.89 ± 0.45	4855 ± 29	60.1 ± 34.4	15.3
	50.38	30.48	65.13 ± 0.71	2.09 ± 0.36	4538 ± 20	−24.2 ± 25.7	10.1
	67.18	45.72	65.13 ± 0.70	2.09 ± 0.35	1261 ± 5.6	− 9.8 ± 7.1	14.1
U II	44.79	15.24	66.73 ± 0.83	2.89 ± 0.42	6176 ± 33	64.2 ± 40.0	11.8
	50.38	30.48	65.39 ± 0.69	2.22 ± 0.35	5784 ± 25	−18.8 ± 31.6	7.3
	67.18	45.72	65.38 ± 0.71	2.21 ± 0.36	1485 ± 6.7	−14.3 ± 8.4	16.4
	67.18	45.72	66.25 ± 0.81	2.65 ± 0.41	1489 ± 7.7	− 0.98 ± 9.5	18.8
U III	44.79	15.24	66.10 ± 0.81	2.57 ± 0.41	7369 ± 39	33.6 ± 47.4	5.8
	50.38	30.48	65.53 ± 0.76	2.29 ± 0.38	6855 ± 33	2.7 ± 41.0	6.4
	67.18	45.72	65.09 ± 0.70	2.07 ± 0.35	1669 ± 7.4	−16.1 ± 9.3	5.8
U IV	44.79	15.24	65.78 ± 0.79	2.41 ± 0.40	7857 ± 40	23.4 ± 49.2	12.2
	50.38	30.48	65.47 ± 0.74	2.26 ± 0.37	7017 ± 33	−25.8 ± 41.4	8.3
	67.18	45.72	64.89 ± 0.68	1.97 ± 0.34	1654 ± 7.1	−18.3 ± 9.0	13.2

TABLE 6

EXTRAPOLATED x – WIDTHS FOR 3RD HARMONIC FITS OF BeO/ThO_2 ASSEMBLIES

Lattice	Position		10.16 cm < x < 50.80 cm				
	z =(cm)	y = (cm)	a_x (cm)	λ_x(cm)	A	B	$\Sigma \frac{\delta^2}{\sigma^2}$
Th Ia	50.38	30.48	66.66 ± 0.86	2.85 ± 0.43	5036 ± 28	25.9 ± 33.8	4.7
	58.78	15.24	66.33 ± 0.83	2.69 ± 0.42	2357 ± 13	8.4 ± 15.4	8.4
	58.78	15.24	65.70 ± 0.77	2.37 ± 0.39	2366 ± 12	− 1.3 ±14.5	8.0
Th II	50.38	30.48	65.87 ± 0.78	2.46 ± 0.39	6010 ± 30	3.2 ± 37.2	11.8
	58.78	15.24	66.05 ± 0.80	2.55 ± 0.40	2716 ± 14	7.4 ± 17.2	9.6
	67.18	45.72	66.35 ± 0.81	2.70 ± 0.41	1571 ± 8.2	1.7 ± 10.0	7.9
Th III	50.38	30.48	64.81 ± 0.73	1.93 ± 0.37	6990 ± 31	−39.7 ± 39.3	13.8
	58.78	15.24	65.58 ± 0.76	2.31 ± 0.38	3018 ± 15	− 2.5 ± 18.2	9.9
	67.18	45.72	65.68 ± 0.74	2.36 ± 0.37	1659 ± 7.8	−10.9 ± 9.7	8.5
Th IV	50.38	30.48	65.11 ± 0.71	2.08 ± 0.36	6302 ± 29	−36.0 ± 35.8	10.9
	58.78	15.24	66.51 ± 0.85	2.78 ± 0.43	2605 ± 14	13.3 ± 17.3	6.3
	67.18	45.72	66.80 ± 0.86	2.92 ± 0.43	1412 ± 7.7	3.4 ± 9.4	14.6

TABLE 7

EXTRAPOLATED y-WIDTHS FOR BeO/UO_2 ASSEMBLIES

Lattice	Range (cm)	z = 41.99 cm x = 45.72 cm			z = 53.18 cm x = 30.48 cm			z = 69.98 cm x = 15.24 cm		
		a_y (cm)	$\Sigma \frac{\delta^2}{\sigma^2}$	No. of Points	a_y (cm)	$\Sigma \frac{\delta^2}{\sigma^2}$	No. of Points	a_y (cm)	$\Sigma \frac{\delta^2}{\sigma^2}$	No. of Points
U Ia	$10.16 \leq y \leq 50.80$	65.43 ± 0.24	9.2	17	66.05 ± 0.24	11.6	17	66.63 ± 0.24	10.5	17
	$12.70 \leq y \leq 48.26$	65.43 ± 0.38	9.1	15	66.11 ± 0.38	10.9	15	66.87 ± 0.38	9.1	15

Lattice	Range (cm)	z = 47.58 cm x = 45.72 cm			z = 58.78 cm x = 15.24 cm			z = 69.98 cm x = 30.48 cm		
		a_y (cm)	$\Sigma \frac{\delta^2}{\sigma^2}$	No. of Points	a_y (cm)	$\Sigma \frac{\delta^2}{\sigma^2}$	No. of Points	a_y (cm)	$\Sigma \frac{\delta^2}{\sigma^2}$	No. of Points
U Ib	$10.16 \leq y \leq 50.80$	65.95 ± 0.24	12.0	17	65.89 ± 0.24	4.4	17	67.00 ± 0.24	4.3	17
	$12.70 \leq y \leq 48.26$	66.28 ± 0.37	10.1	15	66.23 ± 0.37	3.0	15	67.22 ± 0.38	3.5	15
U II	$10.16 \leq y \leq 50.80$	* 66.50 ± 0.26	24.7	14	66.66 ± 0.26	32.4	15	* 67.17 ± 0.28	35.8	14
	$12.70 \leq y \leq 48.26$	* 66.53 ± 0.39	24.6	12	66.56 ± 0.39	32.1	13	* 67.19 ± 0.40	35.7	12
U III	$10.16 \leq y \leq 50.80$	66.17 ± 0.26	10.4	15	66.57 ± 0.26	17.8	15	66.77 ± 0.26	16.5	15
	$12.70 \leq y \leq 48.26$	66.05 ± 0.39	9.9	13	66.60 ± 0.39	17.6	13	66.63 ± 0.39	17.5	13
U IV	$10.16 \leq y \leq 50.80$	66.01 ± 0.26	8.1	15	66.40 ± 0.25	8.9	15	66.57 ± 0.26	29.6	15
	$12.70 \leq y \leq 48.26$	66.06 ± 0.39	7.5	13	66.36 ± 0.39	8.8	13	65.90 ± 0.38	23.4	13

Notes. Observations were not taken at y = 22.86 cm and y = 38.10 cm for Lattices U II, U III, and U IV.

* data at y = 40.64 contributes a $\left(\frac{\delta}{\sigma}\right)^2 > 9$ to total $\Sigma \frac{\delta^2}{\sigma^2}$ which exceeds rejection criterion.

TABLE 8

EXTRAPOLATED y–WIDTHS FOR BeO/ThO_2 ASSEMBLIES

Lattice	Range (cm)	z = 47.58 cm x = 15.24 cm			z = 61.58 cm x = 45.72 cm			z = 69.98 cm x = 30.48 cm		
		a_y (cm)	$\Sigma\frac{\delta^2}{\sigma^2}$	No. of Points	a_y (cm)	$\Sigma\frac{\delta^2}{\sigma^2}$	No. of Points	a_y (cm)	$\Sigma\frac{\delta^2}{\sigma^2}$	No. of Points
Th Ia	$10.16 \leqslant y \leqslant 50.80$	65.94 ± 0.24	13.2	17	65.95 ± 0.24	3.6	17	66.52 ± 0.24	8.6	17
	$12.70 \leqslant y \leqslant 48.26$	65.98 ± 0.38	12.9	15	66.01 ± 0.38	3.5	15	66.56 ± 0.38	8.4	15
Th II	$10.16 \leqslant y \leqslant 50.80$	* 67.44 ± 0.28	20.5	11	◈ 67.17 ± 0.28	13.7	11	67.52 ± 0.28	25.1	12
	$12.70 \leqslant y \leqslant 48.26$	* 67.70 ± 0.47	19.8	9	◈ 67.15 ± 0.43	13.6	9	68.03 ± 0.46	22.6	10
Th III	$10.16 \leqslant y \leqslant 50.80$	66.71 ± 0.26	9.1	12	66.59 ± 0.26	35.0	12	66.48 ± 0.26	12.9	12
	$12.70 \leqslant y \leqslant 48.26$	66.86 ± 0.43	8.6	10	66.72 ± 0.43	33.0	10	66.17 ± 0.43	12.0	10
Th IV	$10.16 \leqslant y \leqslant 50.80$	66.55 ± 0.26	7.0	12	66.94 ± 0.28	10.5	12	66.62 ± 0.28	9.3	12
	$12.70 \leqslant y \leqslant 48.26$	66.46 ± 0.42	6.3	10	66.72 ± 0.43	9.6	10	65.95 ± 0.43	5.4	10

Notes. Measurements were not taken at y = 15.24; 22.86; 30.48; 38.10; 45.72 cm for Lattices ThII, Th III, and Th IV

* data at y = 33.02 contributed $\frac{\delta^2}{\sigma^2} > 9$ which exceeds our rejection criterion.

◈ data at y = 40.64 contributed $\frac{\delta^2}{\sigma^2} > 9$ which exceeds our rejection criterion

TABLE 9

VARIATION OF MEAN N – S WIDTHS (cm) WITH HEIGHT

Position	Lattice				
	U Ia	U Ib	U II	U III	U IV
Bottom	65.43 ± 0.24	65.95 ± 0.24	66.50 ± 0.26	66.17 ± 0.26	66.01 ± 0.26
Middle	66.05 ± 0.24	65.89 ± 0.24	66.66 ± 0.26	66.57 ± 0.26	66.40 ± 0.25
Top	66.63 ± 0.24	67.00 ± 0.24	67.17 ± 0.26	66.77 ± 0.26	66.57 ± 0.26

Position	Lattice			
	Th Ia	Th II	Th III	Th IV
Bottom	65.94 ± 0.24	66.71 ± 0.26	66.55 ± 0.26	67.44 ± 0.28
Middle	65.95 ± 0.24	66.59 ± 0.26	66.94 ± 0.28	67.17 ± 0.28
Top	66.52 ± 0.24	66.48 ± 0.26	66.62 ± 0.28	67.52 ± 0.28

Mean Bottom Width 66.34 ± 0.10 cm

Mean Middle Width 66.48 ± 0.10 cm

Mean Top Width 66.77 ± 0.10 cm

N... W.M. 6.6.53

TABLE 10

VALUES OF RELAXATION LENGTH ($b_{\parallel}$ cm) AND EXTRAPOLATED HEIGHT (h cm)

Lattice		Range 43.8 cm ⩽ z ⩽ 69.1 cm				Range 46.6 cm ⩽ z ⩽ 69.1 cm				Range 49.4 cm ⩽ z ⩽ 69.1 cm				Final Mean
		Centre	$\Sigma\frac{\delta^2}{\sigma^2}$	Corner	$\Sigma\frac{\delta^2}{\sigma^2}$	Centre	$\Sigma\frac{\delta^2}{\sigma^2}$	Corner	$\Sigma\frac{\delta^2}{\sigma^2}$	Centre	$\Sigma\frac{\delta^2}{\sigma^2}$	Corner	$\Sigma\frac{\delta^2}{\sigma^2}$	
UIa	$b_{\parallel}$	17.71 ± 0.20	1.0	17.49 ± 0.20	6.0	17.78 ± 0.27	0.8	17.53 ± 0.26	5.9	17.84 ± 0.36	0.8	17.51 ± 0.34	5.9	17.66 ± 0.18
	h	87.87 ± 0.95		87.87 ± 0.96		87.66 ± 1.05		87.76 ± 1.08		87.51 ± 1.19		87.82 ± 1.27		87.71 ± 0.76
UIb	$b_{\parallel}$	17.35 ± 0.19	10.2	17.59 ± 0.20	7.1	17.65 ± 0.26	6.7	17.54 ± 0.26	7.0	17.72 ± 0.35	6.6	17.96 ± 0.37	3.7	17.60 ± 0.18
	h	87.42 ± 0.91		86.51 ± 0.79		86.58 ± 0.90		86.64 ± 0.91		86.41 ± 1.02		85.73 ± 0.90		86.61 ± 0.65
UII	$b_{\parallel}$	16.34 ± 0.16	12.6	16.44 ± 0.17	5.4	16.67 ± 0.22	6.7	16.59 ± 0.22	4.2	17.00 ± 0.31	3.7	16.90 ± 0.31	1.7	16.63 ± 0.15
	h	87.85 ± 1.03		87.64 ± 0.99		86.65 ± 0.95		87.10 ± 1.02		85.78 ± 0.95		86.21 ± 1.02		86.89 ± 0.72
UIII	$b_{\parallel}$	15.66 ± 0.15	5.2	15.66 ± 0.15	2.0	15.76 ± 0.19	4.4	15.65 ± 0.19	2.0	15.86 ± 0.26	4.1	15.86 ± 0.26	0.4	15.71 ± 0.13
	h	87.47 ± 1.01		91.82 ± 1.94		87.02 ± 1.06		91.93 ± 2.26		86.67 ± 1.15		90.42 ± 2.06		89.48 ± 1.26
UIV	$b_{\parallel}$	15.14 ± 0.13	14.8	15.54 ± 0.14	15.6	15.21 ± 0.17	14.3	15.83 ± 0.19	9.3	15.36 ± 0.23	13.3	16.02 ± 0.26	8.0	15.52 ± 0.13
	h	91.34 ± 1.92		89.75 ± 1.46		90.66 ± 1.95		88.07 ± 1.25		89.61 ± 1.90		87.31 ± 1.27		89.37 ± 1.17
ThIa	$b_{\parallel}$	17.77 ± 0.21	4.0	18.19 ± 0.22	8.4	18.01 ± 0.28	2.0	18.09 ± 0.28	8.0	18.06 ± 0.37	1.9	18.01 ± 0.37	7.9	18.04 ± 0.20
	h	87.41 ± 0.89		86.12 ± 0.72		86.77 ± 0.91		86.34 ± 0.85		86.65 ± 1.04		86.50 ± 1.02		86.56 ± 0.63
Th II	$b_{\parallel}$	16.07 ± 0.16	26.0*	16.59 ± 0.16	6.4	*		16.82 ± 0.23	3.6	17.23 ± 0.32	2.3	16.75 ± 0.30	3.5	16.82 ± 0.23
	h	90.45 ± 1.54		88.24 ± 1.07				87.36 ± 1.05		86.33 ± 1.02		87.60 ± 1.27		87.36 ± 1.05
Th III	$b_{\parallel}$	15.84 ± 0.15	6.8	15.91 ± 0.15	6.3	15.84 ± 0.19	0.7	15.84 ± 0.19	5.0	15.91 ± 0.26	0.5	15.77 ± 0.25	4.8	15.84 ± 0.13
	h	86.65 ± 0.89		86.45 ± 0.85		86.63 ± 1.00		86.77 ± 1.02		86.41 ± 1.11		87.02 ± 1.23		86.70 ± 0.72
Th IV	$b_{\parallel}$	15.29 ± 0.14	7.4	15.62 ± 0.14	8.5	15.52 ± 0.18	3.3	15.80 ± 0.19	6.3	15.39 ± 0.24	2.6	15.99 ± 0.26	4.9	15.66 ± 0.13
	h	87.51 ± 1.05		86.62 ± 0.89		86.51 ± 0.99		85.97 ± 0.90		87.02 ± 1.26		85.41 ± 0.93		86.24 ± 0.68

* Data at z = 46.6 cm contributes $\left(\frac{\delta}{\sigma}\right)^2 > 9$ in both these fits, which exceeds our rejection criterion.

This removes the results from the Range 46.6 ⩽ z ⩽ 69.1 column.

TABLE 11

MEAN VALUES OF EXTRAPOLATED LENGTHS

Lattice	λ_x (cm)	λ_h (cm)	λ_y (cm)
I a	2.45 ± 0.32	3.35 ± 0.77	2.54 ± 0.14
I b	2.35 ± 0.39	2.15 ± 0.66	2.66 ± 0.14
II	2.49 ± 0.39	2.47 ± 0.72	2.91 ± 0.14
III	2.31 ± 0.39	4.82 ± 1.26	2.78 ± 0.14
IV	2.21 ± 0.38	5.12 ± 1.17	2.69 ± 0.14
Th I a	2.64 ± 0.41	2.23 ± 0.64	2.59 ± 0.14
Th II	2.57 ± 0.40	3.60 ± 1.05	3.21 ± 0.14
Th III	2.20 ± 0.37	2.26 ± 0.73	2.82 ± 0.14
Th IV	2.59 ± 0.41	2.11 ± 0.69	2.87 ± 0.14
Overall Mean	$\bar{\lambda}_x$ = 2.42 ± 0.25	$\bar{\lambda}_h$ = 3.12 ± 0.29	$\bar{\lambda}_y$ = 2.79 ± 0.10

Measured Stack Dimensions (All Lattices)

E – W (x) cm	60.96 ± 0.10 cm
N – S (y) cm	60.96 ± 0.10 cm
Height (z) cm	84.40 ± 0.10 cm

2.42 .25 .0625 .16 00
3.12 .29 .0841 .11 89
2.79 .10 .0100 100 00

2.77 ± 0.09

TABLE 12

THE MATERIALS BUCKLINGS

Lattice	$\left(\frac{\pi}{a_x}\right)^2$ (m^{-2})	$\left(\frac{\pi}{a_y}\right)^2$ (m^{-2})	$\left(\frac{1}{b_{II}}\right)^2$ (m^{-2})	K^2 (m^{-2})($M_{II}^2/M_{\perp}^2$) = 1	K^2(m^{-2})$\left(M_{II}^2/M_{\perp}^2\right)$ from Keane
U Ia	22.78 ± 0.25	22.30 ±0.15	32.06 ±0.65	13.0 ± 0.8	13.3
U Ib	22.78 ±0.25	22.30 ±0.15	32.28 ±0.66	12.8 ±0.8	13.1
U II	22.78 ±0.25	22.30 ± 0.15	36.16 ±0.65	8.9 ±0.8	9.7
U III	22.78 ± 0.25	22.30 ±0.15	40.52 ±0.67	4.5 ±0.8	5.8
U IV	22.78 ± 0.25	22.30 ±0.15	41.52 ±0.70	3.5 ±0.8	5.1
Th Ia	22.78 ±0.25	22.30 ±0.15	30.73 ±0.68	14.3 ±0.8	14.6
Th II	22.78 ±0.25	22,30 ±0.15	35.35 ±0.68	9,7 ±0.8	10.5
Th III	22,78 ±0.25	22.30 ±0.15	39.86 ±0.65	5.2 ±0.8	6.5
Th IV	22.78 ±0.25	22.30 ±0.15	40.78 ±0.68	4.3 ±0.8	5.8

TABLE 13

MEASURED FISSION RATIOS

U235/U238/BeO Lattices

Lattice Number	Fission Ratio per Fissile Atom	
	Pu239/U235	U233/U235
I a	1.935 ± 0.032	1.137 ± 0.019
I b	1.938 ± 0.032	1.139 ± 0.019
II	1.699 ± 0.027	1.047 ± 0.017
III	1.670 ± 0.028	1.044 ± 0.018
IV	1.624 ± 0.027	1.014 ± 0.017

U235/Th232/BeO Lattices

Lattice Number	Fission Ratio per Fissile Atom	
	Pu239/U235	U233/U235
I a	1.978 ± 0.033	1.153 ± 0.019
II	1.792 ± 0.031	1.067 ± 0.019
III	1.705 ± 0.029	1.041 ± 0.018
IV	1.601 ± 0.027	1.005 ± 0.017

TABLE 14

COMPARISON OF EXPERIMENTAL RESULTS WITH CALCULATIONS

(a) Materials Buckling

Mills (Los Alamos)

Lattice	Expt. B_m^2 (m^{-2}) $\frac{M_{II}^2}{M_\perp^2} = 1$	Expt. B_m^2 (m^{-2}) $\frac{M_{II}^2}{M_\perp^2}$ from Keane	Calculated B_m^2 (m^{-2})	LH data
U Ia	13.0 ± 0.8	13.3	12.5	8.4
U Ib	12.8 ± 0.8	13.1	12.5	6.6
U II	8.9 ± 0.8	9.7	10.5	3.0
U III	4.5 ± 0.8	5.8	6.9	
U IV	3.5 ± 0.8	5.1 ± 0.8	4.8	0.8
Th Ia	14.3 ± 0.8	14.6	11.5	13.3
Th II	9.7 ± 0.8	10.5	9.0	8.4
Th III	5.2 ± 0.8	6.5	4.0	4.0
Th IV	4.3 ± 0.8	5.8	1.1	0.6

(b) Fission Ratios

Lattice	Pu239/U235			U233/U235		
	Calculated	Experimental	$\frac{\text{Calculated}}{\text{Experimental}}$	Calculated	Experimental	$\frac{\text{Calculated}}{\text{Experimental}}$
U Ia	2.503	1.935 ± 0.032	1.29	1.263	1.137 ± 0.019	1.11
U Ib	2.503	1.938 ± 0.032	1.29	1.263	1.139 ± 0.019	1.11
U II	2.331	1.699 ± 0.027	1.37	1.196	1.047 ± 0.017	1.14
U III	2.096	1.670 ± 0.028	1.26	1.113	1.044 ± 0.018	1.07
U IV	1.993	1.624 ± 0.027	1.23	1.081	1.014 ± 0.017	1.07
Th Ia	2.454	1.978 ± 0.033	1.24	1.239	1.153 ± 0.019	1.08
Th II	2.272	1.792 ± 0.031	1.27	1.172	1.067 ± 0.019	1.09
Th III	2.021	1.705 ± 0.029	1.18	1.091	1.041 ± 0.018	1.05
Th IV	1.917	1.601 ± 0.027	1.20	1.062	1.005 ± 0.017	1.06

TABLE 15

COMPARISON OF EXPERIMENTAL RESULTS REPORTED BY DUERDEN ET AL. (1964) WITH CALCULATIONS

Materials Buckling

Lattice	Expt. B_m^2 (m^{-2})	Calc. B_m^2 (m^{-2})
1	54.9 ± 1.8	55.2
2	45.0 ± 1.6	44.2
3	33.2 ± 1.0	35.2
4	22.8 ± 1.0	27.5

Fission Ratios

	Pu239/U235			U233/U235		
Lattice	Calculated	Experimental	Calculated / Experimental	Calculated	Experimental	Calculated / Experimental
1	2.53	2.12 ± 0.05	1.19	1.27	1.26 ± 0.03	1.01
2	2.23	1.86 ± 0.05	1.20	1.16	1.10 ± 0.03	1.05
3	1.99	1.67 ± 0.04	1.19	1.08	1.03 ± 0.03	1.05
4	1.89	1.56 ± 0.04	1.21	1.05	1.03 ± 0.03	1.02

APPENDIX 1

Mean Fuel Strip Data

Dimensions: 24.0in x 1.330in x 0.040in

Composition: Aluminium 53.11 g

Uranium 16.24 g

Isotopic Composition of Uranium (atom per cent.)

U234	U235	U236	U238
1.00	89.41	3.28	6.31

APPENDIX 2

(a) Mean BeO/UO_2 Slab Data

Dimensions: 24.0in x 24.0in x 1.00in

Weight: 15.658 kg

Uranium content: 4.31 per cent. by weight (natural uranium)

(b) Aluminium Container

Material: 99.0 per cent. pure aluminium

Top Plate Dimension: 24.5in x 24.5in x 0.080in – weight 1214 g

Bottom Plate Dimension: 24.5in x 24.5in x 0.022in – weight 610 g

APPENDIX 3

(a) Mean BeO/ThO_2 Slab Data

Dimensions: 24.0in x 24.0in x 1.00in

Weight: 15.804 kg

Thorium Content: 4.32 per cent. by weight

(b) Aluminium Container

Material: 99.5 per cent. pure aluminium

Top Plate Dimension: 24.5in x 24.5in x 0.080in – weight 1214 g

Bottom Plate Dimensions: 24.5in x 24.5in x 0.022in – weight 610 g

APPENDIX 4

VERTICAL (z) FLUX SCANS FOR BeO/UO_2 ASSEMBLIES

x = (cm)		Lattice U Ia		Lattice U Ib		Lattice U II		Lattice U III		Lattice U IV	
		35.56	20.32	35.56	20.32	35.56	20.32	35.56	20.32	35.56	20.32
y = (cm)		35.56	20.32	35.56	20.32	35.56	20.32	35.56	20.32	35.56	20.32
z (in)	z (cm)	ϕ	ϕ	ϕ	ϕ	ϕ	ϕ	ϕ	ϕ	ϕ	ϕ
2	71.88	721.4	607.3	720,5	623.8	798.0	642.0	1003	837	1110	917.8
3	69.08	913.5	752.5	910.0	776.0	998.0	812.0	1254	1051	1418	1158
4	66.28	1110	917.4	1107	949.0	1215	996.0	1562	1284	1719	1415
5	63.48	1337	1105	1337	1147	1491	1217	1912	1552	2114	1736
6	60.69	1593	1323	1611	1377	1793	1457	2308	1867	2587	2114
7	57.89	1891	1549	1930	1650	2162	1755	2766	2249	3057	2495
8	55.09	2229	1867	2245	1932	2565	2085	3348	2694	3742	3047
9	52.29	2621	2181	2659	2270	3037	2468	4003	3234	4535	3638
10	49.49	3103	2589	3158	2697	3602	2947	4839	3854	5368	4325
11	46,69	3641	3038	3711	3208	4336	3533	5789	4665	6552	5230
12	43.89	4284	3581	4427	3737	5213	4203	6962	5550	7898	6359
13	41.09	5112	4229	5237	4362	6229	5081	8358	6797	9308	7530
14	38.29	6075	5029		✓						

APPENDIX 5

EAST–WEST (x) FLUX SCANS FOR BeO/UO_2 ASSEMBLIES

		Lattice U Ia			Lattice U Ib			Lattice U II				Lattice U III			Lattice U IV		
z = (cm)		39.19	50.38	67.18	44.79	50.38	67.18	44.79	50.38	67.18		44.79	50.38	67.18	44.79	50.38	67.18
y = (cm)		15.24	30.48	45.72	15.24	30.48	45.72	15.24	30.48	45.72		15.24	30.48	45.72	15.24	30.48	45.72
x (in)	x (cm)	ϕ	ϕ	ϕ	ϕ	ϕ	ϕ	ϕ	ϕ	ϕ		ϕ	ϕ	ϕ	ϕ	ϕ	ϕ
4	10.16	3861	2597	700.1	2708	2534	703.8	3465	3216	851.3	836.8	4079	3768	933.0	4386	3948	926.7
5	12.70	4580	3035	815.8	3172	2970	835.1	4071	3800	985.4	968.4	4809	4451	1098	5177	4646	1098
6	15.24	5148	3445	919.6	3627	3377	935.2	4569	4288	1113	1097	5467	5028	1242	5868	5216	1236
7	17.78	5703	3806	1026	3986	3683	1038	5104	4707	1221	1220	5994	5582	1361	6411	5757	1363
8	20.32	6154	4091	1099	4294	3991	1113	5473	5104	1324	1310	6455	6008	1467	6929	6185	1458
9	22.86	6489	4294	1168	4516	4220	1174	5781	5366	1384	1388	6857	6368	1559	7393	6529	1536
10	25.40	6807	4444	1211	4741	4375	1219	6043	5592	1448	1427	7180	6631	1605	7684	6776	1589
11	27.94	6940	4565	1244	4886	4482	1243	6208	5730	1478	1451	7317	6830	1635	7761	6943	1627
12	30.48	7058	4582	1257	4903	4524	1247	6234	5784	1477	1467	7386	6846	1651	7869	7016	1641
13	33.02	6999	4576	1241	4890	4504	1240	6161	5718	1472	1452	7388	6809	1647	7818	6942	1620
14	35.56	6830	4487	1218	4799	4375	1217	6068	5588	1452	1443	7232	6679	1604	7633	6772	1592
15	38.10	6550	4349	1176	4629	4239	1178	5852	5431	1392	1387	6945	6405	1553	7417	6583	1528
16	40.64	6212	4082	1114	4304	3988	1106	5494	5115	1324	1316	6546	6146	1473	6953	6209	1466
17	43.18	5715	3804	1040	4003	3734	1029	5134	4746	1237	1227	6109	5647	1377	6448	5715	1347
18	45.72	5194	3453	936.5	3661	3403	939.1	4673	4360	1128	1124	5563	5164	1248	5837	5269	1227
19	48.26	4613	3069	827.3	3225	3034	842.0	4096	3859	980.0	995.6	4932	4588	1113	5175	4662	1097
20	50.80	3922	2616	716.1	2770	2557	717.5	3534	3287	855.2	860.1	4228	3925	956.0	4444	3964	940.6
		Bottom	Centre	Top	Bottom	Centre	Top	Bottom	Centre	Top		Bottom	Centre	Top	Bottom	Centre	Top

APPENDIX 6

N – S (y) FLUX SCANS FOR UO_2/BeO ASSEMBLIES

(a) Lattices U Ia and U Ib . Observed Fluxes y-direction

	Lattice U Ia			Lattice U Ib		
z (cm)	41.99	53.18	69.98	47.58	58.78	69.98
x (cm)	45.72	30.48	15.24	45.72	15.24	30.48
y (cm)	Observed Fluxes					
10.16	3124	2184	576.4	2344	1221	769.4
12.70	3687	2508	671.5	2735	1432	897.5
15.24	4189	2860	759.7	3095	1612	1011
17.78	4672	3142	840.0	3419	1776	1104
20.32	4988	3365	899.0	3716	1910	1186
22.86	5316	3563	947.1	3864	2023	1250
25.40	5563	3699	976.7	4071	2087	1279
27.94	5711	3828	999.0	4120	2136	1321
30.48	5764	3864	999.3	4144	2144	1333
33.02	5695	3858	997.5	4115	2131	1317
35.56	5578	3770	982.8	4048	2099	1297
38.10	5349	3612	948.5	3850	2004	1245
40.64	5135	3433	896.5	3673	1907	1182
43.18	4730	3183	833.2	3446	1777	1098
45.72	4326	2906	758.1	3124	1602	1006
48.26	3882	2615	679.6	2795	1433	892.2
50.80	3312	2225	581.0	2355	1210	768.9

(continued)

APPENDIX 6 (continued)

(b) Lattice U II. Observed and corrected fluxes y – direction

y cm	x = 30.48 cm z = 69.98 cm		x = 15.24 cm z = 58.78 cm		x = 45.72 cm z = 47.58 cm	
	Observed Flux	Corrected Flux	Observed Flux	Corrected Flux	Observed Flux	Corrected Flux
10.16	834.5	893.0	1361	1456	2715	2905
12.70	1031	1049	1678	1707	3354	3412
15.24	1175	1175	1919	1919	3836	3836
17.78	1252	1274	2065	2101	4104	4175
20.32	1266	1355	2080	2226	4176	4469
25.40	1392	1489	2306	2468	4672	5000
27.94	1530	1556	2517	2560	4998	5084
30.48	1568	1568	2589	2589	5190	5190
33.02	1555	1582	2539	2583	5100	5188
35.56	1435	1536	2369	2535	4685	5013
40.64	1268	1357	2094	2241	4145	4436
43.18	1254	1276	2066	2102	4115	4186
45.72	1183	1183	1941	1941	3899	3899
48.26	1052	1070	1716	1746	3451	3510
50.80	859.0	919.0	1400	1498	2794	2990

(continued)

APPENDIX 6 (continued)

(c) Lattice U III. Observed and corrected fluxes y – direction

y cm	x = 30.48 cm z = 69.98 cm		x = 15.24 cm z = 58.78 cm		x = 45.72 cm z = 47.58 cm	
	Observed Flux	Corrected Flux	Observed Flux	Corrected Flux	Observed Flux	Corrected Flux
10.16	934	971.5	1587	1651	3303	3435
12.70	1131	1143	1919	1939	3991	4032
15.24	1281	1281	2154	2154	4545	4545
17.78	1380	1394	2349	2373	4932	4982
20.32	1422	1479	2438	2536	5144	5350
25.40	1577	1640	2689	2797	5694	5922
27.94	1673	1690	2833	2862	6009	6070
30.48	1715	1715	2907	2907	6128	6128
33.02	1683	1700	2875	2904	6059	6121
35.56	1611	1676	2741	2851	5742	5972
40.64	1451	1509	2439	2537	5160	5367
43.18	1383	1397	2348	2372	4955	5007
45.72	1281	1281	2190	2190	4577	5006
48.26	1131	1143	1935	1955	4074	4116
50.80	954	992.3	1603	1667	3391	3527

(continued)

APPENDIX 6 (continued)

(d) Lattice U IV. Observed and corrected fluxes y – direction

y cm	x = 30.48 cm z = 69.98 cm		x = 15.24 cm z = 58.78 cm		x = 45.72 z = 47.58 cm	
	Observed Flux	Corrected Flux	Observed Flux	Corrected Flux	Observed Flux	Corrected Flux
10.16	955.5	993.8	1653	1719	3426	3563
12.70	1136	1148	1993	2013	4183	4226
15.24	1294	1294	2263	2263	4761	4761
17.78	1408	1422	2461	2486	5159	5212
20.32	1506	1566	2572	2675	5395	5611
25.40	1640	1706	2826	2935	6013	6254
27.94	1690	1707	2994	3025	6293	6358
30.48	1726	1726	3040	3040	6425	6425
33.02	1704	1721	3002	3033	6336	6401
35.56	1655	1722	2850	2964	6079	6323
40.64	1494	1554	2554	2653	5525	5747
43.16	1412	1426	2477	2502	5236	5289
45.72	1298	1298	2300	2300	4851	4851
48.26	1154	1166	2018	2039	4296	4340
50.80	978.6	1018	1686	1754	3590	3734

APPENDIX 7

VERTICAL (z) FLUX SCANS FOR BeO/ThO_2 ASSEMBLIES

		Lattice Th I		Lattice Th II		Lattice Th III		Lattice Th IV	
x = (cm)		35.56	20.32	35.56	20.32	35.56	20.32	35.56	20.32
y = (cm)		35.56	20.32	35.56	20.32	35.56	20.32	35.56	20.32
z (in)	z (cm)	ϕ	ϕ	ϕ	ϕ	ϕ	ϕ	ϕ	ϕ
2	71.88	894.0	735.2	895.0	733.1	1084	910.2	1135	987.0
3	69.08	1114	910.5	1114	906.0	1367	1160	1427	1243
4	66.28	1353	1124	1366	1117	1688	1439	1768	1541
5	63.48	1623	1336	1656	1347	2063	1749	2171	1896
6	60.69	1956	1604	1992	1605	2507	2114	2647	2297
7	57.89	2315	1921	2365	1941	3034	2590	3182	2773
8	55.09	2730	2238	2843	2305	3636	3072	3856	3353
9	52.29	3218	2635	3334	2729	4371	3721	4689	4052
10	49.49	3765	3135	3962	3260	5215	4439	5592	4767
11	46.69	4435	3647	4877	3842	6269	5303	6690	5800
12	43.89	5257	4255	5760	4620	7486	6313	8194	6994
13	41.09	6090	5035	6908	5523	9149	7662	9685	8345

APPENDIX 8

EAST – WEST (x) FLUX SCANS FOR BeO/ThO_2 ASSEMBLIES

		Lattice Th Ia			Lattice Th II			Lattice Th III			Lattice Th IV		
z = (cm)		50.38	58.78		50.38	58.78	67.18	50.38	58.78	67.18	50.38	58.78	67.18
y = (cm)		30.48	15.24		30.48	15.24	45.72	30.48	15.24	45.72	30.48	15.24	45.72
x (in)	x (cm)	ϕ	ϕ		ϕ	ϕ	ϕ	ϕ	ϕ	ϕ	ϕ	ϕ	ϕ
4	10.16	2867	1327	1321	3357	1507	884.7	3887	1672	939.2	3584	1483	812.4
5	12.70	3331	1545	1545	3942	1770	1034	4519	1962	1091	4213	1746	945.4
6	15.24	3765	1751	1751	4458	2021	1173	5185	2235	1245	4722	1964	1057
7	17.78	4133	1930	1934	4923	2208	1293	5735	2467	1359	5187	2151	1174
8	20.32	4492	2096	2086	5303	2395	1390	6159	2662	1464	5588	2315	1255
9	22.86	4725	2200	2185	5613	2521	1473	6494	2790	1549	5884	2450	1336
10	25.40	4894	2287	2278	5844	2653	1532	6746	2920	1599	6130	2532	1376
11	27.94	5026	2333	2346	5971	2680	1560	6929	3009	1646	6256	2598	1416
12	30.48	5074	2363	2369	5994	2732	1574	6922	3012	1644	6253	2627	1409
13	33.02	5022	2357	2353	5963	2720	1561	6839	2991	1626	6144	2605	1397
14	35.56	4910	2302	2304	5850	2641	1525	6787	2936	1606	6107	2546	1367
15	38.10	4712	2211	2221	5624	2556	1470	6530	2819	1547	5849	2429	1324
16	40.64	4490	2104	2112	5361	2416	1392	6169	2670	1462	5525	2303	1250
17	43.18	4164	1966	1956	4925	2247	1294	5730	2512	1367	5132	2137	1167
18	45.72	3803	1778	1782	4522	2046	1183	5181	2265	1250	4636	1947	1066
19	48.26	3349	1566	1567	4007	1823	1060	4616	2003	1108	4122	1718	936.3
20	50.80	2884	1349	1362	3440	1563	907.3	3937	1733	953.8	3493	1477	813.2

APPENDIX 9

N–S (y) FLUX SCANS FOR BeO/ThO_2 ASSEMBLIES

(a) Lattice Th Ia. Observed fluxes y – direction

y (cm)	z = 47.58 cm x = 15.24 cm	z = 61.58 cm x = 45.72 cm	z = 69.98 cm x = 30.48 cm
	Observed Fluxes		
10.16	2507	1540	842.1
12.70	2912	1814	983.0
15.24	3329	2057	1122
17.78	3670	2262	1228
20.32	3977	2437	1309
22.86	4128	2586	1380
25.40	4295	2688	1442
27.94	4442	2755	1480
30.48	4508	2790	1487
33.02	4447	2771	1479
35.56	4407	2708	1459
38.10	4295	2592	1411
40.64	4040	2463	1342
43.18	3732	2292	1243
45.72	3395	2094	1129
48.26	3018	1871	1015
50.80	2591	1609	865.0

(continued)

APPENDIX 9 (continued)

(b) Lattice Th II. Observed and corrected fluxes y – direction

y cm	x = 30.48 cm z = 69.98 cm		x = 45.72 cm z = 61.58 cm		x = 15.24 cm z = 47.58 cm	
	Observed Flux	Corrected Flux	Observed Flux	Corrected Flux	Observed Flux	Corrected Flux
10.16	901.4	964.6	1774	1898	2872	3073
12.70	1121	1140	2204	2242	3538	3599
17.78	1348	1372	2721	2769	4315	4389
20.32	1359	1454	2731	2922	4335	4639
25.40	1499	1604	3011	3222	4806	5143
27.94	1627	1655	3307	3364	5227	5317
33.02	1645	1673	3297	3354	5322	5414
35.56	1512	1618	3039	3252	4880	5222
40.64	1355	1450	2691	2880	4350	4655
43.18	1341	1364	2690	2734	4273	4346
48.26	1109	1128	2245	2284	3558	3619
50.80	903.7	967.0	1835	1964	2899	3102

(c) Lattice Th III. Observed and corrected fluxes y – direction

y cm	x = 30.48 cm z = 69.98 cm		x = 45.72 cm z = 61.58 cm		x = 15.24 cm z = 47.58 cm	
	Observed Flux	Corrected Flux	Observed Flux	Corrected Flux	Observed Flux	Corrected Flux
10.16	861.4	886.9	1924	1981	3400	3501
12.70	1038	1038	2325	2325	4122	4122
17.78	1256	1256	2906	2906	5090	5090
20.32	1310	1349	2998	3087	5281	5437
25.40	1466	1509	3305	3403	5811	5983
27.94	1539	1539	3563	3563	6232	6232
33.02	1536	1536	3542	3542	6214	6214
35.56	1460	1503	3339	3438	5906	6081
40.64	1321	1360	2971	3059	5341	5499
43.18	1263	1263	2910	2910	5162	5162
48.26	1021	1021	2420	2420	4242	4242
50.80	857.8	883.2	2007	2066	3546	3651

(continued)

APPENDIX 9 (continued)

(d) Lattice Th IV. Observed and corrected fluxes y – direction

y cm	x = 30.48 cm, z = 69.98 cm		x = 45.72 cm, z = 61.58 cm		x = 15.24 cm, z = 47.58 cm	
	Observed Flux	Corrected Flux	Observed Flux	Corrected Flux	Observed Flux	Corrected Flux
10.16	845.7	870.7	1751	1803	3124	3216
12.70	998.3	998.3	2096	2096	3772	3772
17.78	1224	1224	2544	2544	4569	4569
20.32	1291	1329	2663	2742	4786	4928
25.40	1415	1457	2952	3039	5275	5431
27.94	1485	1485	3076	3076	5579	5575
33.02	1480	1480	3049	3049	5537	5537
35.56	1408	1450	2912	2998	5227	5382
40.64	1282	1320	2633	2711	4792	4934
43.18	1207	1207	2500	2500	4545	4545
48.26	985.2	985.2	2052	2052	3683	3683
50.80	826.9	851.4	1716	1767	3087	3178

APPENDIX 10

CADMIUM RATIOS FOR BeO/UO_2 ASSEMBLIES

(a) Horizontal

Posn.	Lattice U Ia						Lattice U II		Lattice U III		Lattice U IV	
	E–W	E–W	E–W	N–S	N–S	N–S	E–W	N–S	E–W	E–W	N–S	E–W
	B/L	C/C	T/R	B/R	C/C	T/L	B/L	T/C	B/L	C/C	B/R	T/R
4	7.39	6.82	6.73	6.75	6.65	6.58	9.96	8.85	14.54	14.69	18.05	15.95
5	7.28	6.79	6.77	6.81	6.75	6.83	9.98	9.46	14.57	14.56	18.44	16.73
6	7.22	6.87	6.86	6.94	6.75	6.94	10.04	9.33	15.12	14.57	19.07	16.32
8	7.30	6.81	6.74	6.92	6.56	6.85	9.62	8.67	15.29	14.98	18.27	16.53
10	7.45	6.79	6.90	7.03	6.75	6.76	10.19	8.87	15.16	15.17	17.77	16.67
12	7.42	6.78	6.93	7.03	6.61	6.63	10.03	9.56	15.17	15.24	18.90	16.61
14	7.27	6.87	6.93	6.89	6.79	6.91	9.79	9.14	15.27	15.11	18.43	17.27
16	7.35	6.90	6.89	6.99	6.66	6.67	10.14	8.74	14.95	15.67	18.14	16.79
18	7.26	6.70	6.80	7.03	6.70	6.68	9.88	9.54	15.29	14.96	18.54	16.60
19	7.22	6.65	6.66	6.95	6.51	6.65	9.73	9.48	14.88	15.44	18.10	16.47
20	7.16	6.71	6.69	6.99	6.63	6.62	9.87	9.15	15.17	14.81	18.11	16.30
		6.79	6.80	6.93	6.66	6.73	9.93	9.16	15.03	15.01	18.3	16.6

(b) Vertical

Posn.	Lattice U Ia		Lattice U II	Lattice U III	Lattice U IV
	Centre	Corner	Centre	Centre	Centre
2	6.75	6.89	9.16	12.90	15.36
3	6.98	6.87	9.21	13.07	15.90
4	6.93	6.86	8.87	13.10	15.45
5			9.12	13.31	15.16
6	6.56	6.52	9.14	12.77	15.70
7			9.08	12.98	15.15
8	6.76	6.57	9.12	12.93	15.36
9			9.37	13.30	15.81
10	6.85	6.75	9.14	13.04	15.18
11			9.31	13.17	15.43
12	6.90	6.82	9.60	13.18	15.66
13	7.08	6.99	9.88	13.49	15.05
14	7.24	7.17			
	6.89	6.82	9.25	13.1	

Mean 6.80

APPENDIX 11

CADMIUM RATIOS FOR BeO/ThO_2 ASSEMBLIES

(a) Horizontal

Posn.	Lattice Th Ia		Lattice Th II		Lattice Th III		Lattice Th IV	
	E – W	N – S	E – W	E – W	E – W	E – W	E – W	E – W
	B/C	T/C	B/C	T/R	B/C	T/R	B/C	T/R
4	6.76	6.64	9.98	9.50	14.85	13.87	19.76	17.82
5	6.77	6.80	9.69	9.48	14.97	14.05	19.95	18.36
6	6.71	6.72	9.78	9.89	15.28	14.09	19.94	18.29
8	6.68	6.71	10.14	9.75	15.30	14.40	20.52	17.72
10	6.78	6.71	9.69	9.82	15.27	14.00	19.87	18.26
12	6.85	6.98	10.04	9.73	14.87	14.18	19.55	18.33
14	6.78	7.01	10.16	9.78	15.25	14.32	19.95	17.53
16	6.75	6.97	9.89	9.33	15.08	14.07	19.65	17.87
18	6.79	6.60	10.06	9.44	14.80	13.85	19.61	17.58
19	6.70	6.95	10.08	9.72	14.95	13.56	19.17	17.49
20	6.57	6.50	9.90	9.39	14.72	13.84	19.26	17.68
	6.74	6.78	9.95	9.62	15.0	14.0	19.7	17.9

(b) Vertical

Posn.	Lattice Th Ia		Lattice Th II	Lattice Th III	Lattice Th IV
	Centre	Corner	Centre	Centre	Centre
2	5.59	6.89	9.38	13.61	16.57
3	5.41	6.94	9.25	13.22	17.07
4	5.43	7.11	9.05	13.65	16.83
5	5.36	6.87	9.03	13.67	16.50
6	5.41	6.99	9.15	13.08	16.49
7	5.46	6.82	9.33	13.50	16.26
8	5.34	6.94	9.01	13.20	16.31
9	5.34	6.88	9.11	13.71	16.52
10	5.42	6.79	9.29	13.58	16.34
11	5.34	6.76	9.69	13.66	16.09
12	5.52	6.91	9.65	13.76	15.98
13	5.47	7.19	10.13	13.98	15.96
	5.42	6.92			

LATTICE CELL

LATTICE II

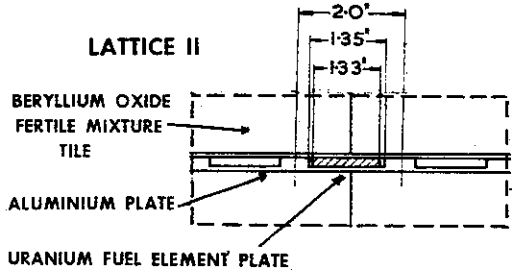

LATTICE III

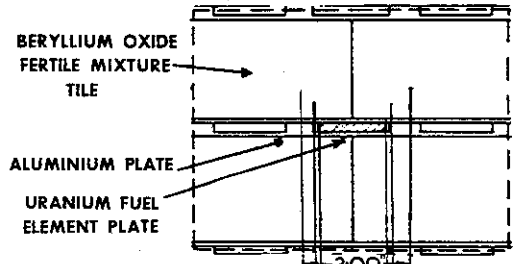

LATTICE IV

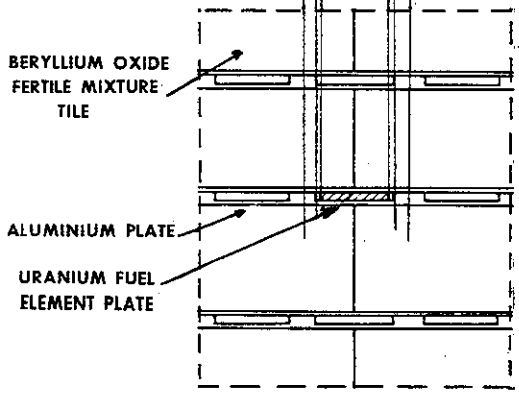

CELL STRUCTURE USED FOR FINE STRUCTURE CALCULATIONS

LATTICE II

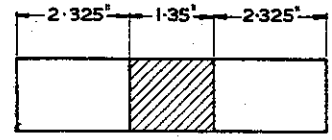

LATTICES III & IV

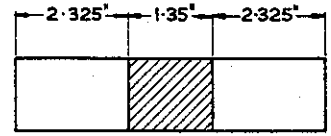

The effect of fuel elements at distances equal to or greater than 1.5 inches was neglected

ATOMIC DENSITIES USED IN FINE STRUCTURE CALCULATIONS

LATTICE U II

BeO	$3{\cdot}436 \times 10^{22}$	atoms /cc throughout
Al	$4{\cdot}160 \times 10^{21}$	atoms /cc throughout
O	$2{\cdot}60 \times 10^{20}$	atoms /cc throughout
U_{235}	$1{\cdot}162 \times 10^{18}$	atoms /cc in unshaded area
	$6{\cdot}454 \times 10^{19}$	atoms /cc in shaded area
U_{238}	$1{\cdot}629 \times 10^{20}$	atoms /cc in unshaded area
	$1{\cdot}674 \times 10^{20}$	atoms /cc in shaded area

LATTICE Th II

BeO	$3{\cdot}474 \times 10^{22}$	atoms/cc throughout
Al	$4{\cdot}179 \times 10^{21}$	atoms/cc throughout
O	$3{\cdot}700 \times 10^{20}$	atoms/cc throughout
Th	$1{\cdot}703 \times 10^{20}$	atoms/cc throughout
U_{235}	$6{\cdot}338 \times 10^{19}$	atoms/cc in shaded area only
U_{238}	$2{\cdot}325 \times 10^{18}$	atoms/cc in shaded area only

LATTICES U III & U IV

BeO	$3{\cdot}436 \times 10^{22}$	atoms /cc throughout
Al	$3{\cdot}931 \times 10^{21}$	atoms /cc throughout
O	$2{\cdot}50 \times 10^{20}$	atoms /cc throughout
U_{235}	$1{\cdot}162 \times 10^{18}$	atoms /cc in unshaded area
	$3{\cdot}285 \times 10^{19}$	atoms /cc in shaded area
U_{238}	$1{\cdot}629 \times 10^{20}$	atoms /cc in unshaded area
	$1{\cdot}651 \times 10^{20}$	atoms /cc in shaded area

LATTICES Th III & Th IV

BeO	$3{\cdot}474 \times 10^{22}$	atoms/cc throughout
Al	$3{\cdot}950 \times 10^{21}$	atoms/cc throughout
O	$3{\cdot}600 \times 10^{20}$	atoms/cc throughout
Th	$1{\cdot}703 \times 10^{20}$	atoms/cc throughout
U_{235}	$3{\cdot}169 \times 10^{19}$	atoms/cc in shaded area only
U_{238}	$2{\cdot}325 \times 10^{18}$	atoms/cc in shaded area only

The effect of fuel elements at distances equal to or greater than 1.5 inches was neglected

APPENDIX 12 CELL STRUCTURE USED FOR FINE STRUCTURE CALCULATIONS

APPENDIX 13

FINE STRUCTURE CORRECTION FACTORS USED IN N – S (y) WIDTH ANALYSIS

Lattice	y (cm)	Correction Factor
U II and Th II	15.24, 30.48, 45.72	1.0000
	12.70, 17.78, 27.94, 33.02, 43.18, 48.26	1.0172
	10.16, 20.32, 25.40, 35.56, 40.64, 50.80	1.0701
	22.86, 38.10	1.1012
Th III, Th IV U III, Th III	15.24, 30.48, 45.72	1.0000
	12.70, 17.78, 27.94, 33.02, 43.18, 48.26	1.0102
	10.16, 20.32, 25.40, 35.56, 40.64, 50.80	1.0401
	22.86, 38.10	1.0564
Th III, Th IV U III, Th III *	12.70, 17.78, 27.94, 33.02, 43.18, 48.26	1.0000
	10.16, 20.32, 25.40, 35.56, 40.64, 50.80	1.0296

* These correction factors were used for scans in which positions 15.24, 22.86, 30.48, 38.10, and 45.72 were omitted.

APPENDIX 14

RELATIVE FISSION RATES IN THE URANIA LATTICES

		Lattice U Ia	Lattice U Ib	Lattice U II	Lattice U III	Lattice U IV
U235	Count Rate in Lattice	1.000 ± 0.011	1.000 ±0.011	1.000 ±0.011	1.000 ±0.010	1.000 ±0.009
	Count Rate in Thermal Column	1.000 ± 0.006	1.000 ±0.006	1.000 ±0.006	1.000 ±0.006	1.000 ±0.006
	Effective number of fissile atoms	1.000 ± 0.012	1.000 ±0.012	1.000 ±0.012	1.000 ±0.012	1.000 ±0.012
U233	Count Rate in Lattice	0.341 ±0.004	0.341 ±0.004	0.324 ±0.003	0.332 ±0.003	0.323 ±0.003
	Count Rate in Thermal Column	0.280 ±0.002	0.280 ±0.002	0.290 ±0.002	0.297 ±0.002	0.297 ±0.002
	Effective number of fissile atoms	0.300 ±0.004	0.300 ±0.004	0.310 ±0.004	0.318 ±0.004	0.318 ±0.004
Pu239	Count Rate in Lattice	0.169 ±0.002	0.169 ±0.002	0.153 ±0.002	0.153 ±0.002	0.149 ±0.002
	Count Rate in Thermal Column	0.121 ±0.001	0.121 ±0.001	0.124 ±0.001	0.127 ±0.001	0.127 ±0.001
	Effective number of fissile atoms	0.0872 ±0.0010	0.0872 ±0.0010	0.0898 ±0.0010	0.0917 ±0.0010	0.0917 ±0.0010

Relative effective number of fissile atoms for each chamber were calculated using effective 20.44°C Maxwellian average cross sections given by Westcott (1960)

viz. σ_{f5} = 563.1 b σ_{f3} = 525.2 b σ_{f9} = 778.3 b

APPENDIX 15

RELATIVE FISSION RATIOS IN THE THORIA LATTICES

Counter	Lattice Th Ia	Lattice Th II	Lattice Th III	Lattice Th IV	Thermal	Relative Effective Number of Fissile Atoms
U235	1.000 ±0.011				1.000 ±0.007	1.000 ±0.012
U233	0.363 ±0.004				0.294 ±0.002	0.315 ±0.004
Pu239	0.181 ±0.002				0.127 ±0.001	0.0916 ±0.0011
U235		1.000 ±0.011	1.000 ±0.011	1.000 ±0.011	1.000 ±0.006	1.000 ±0.012
U233		0.340 ±0.004	0.331 ±0.003	0.320 ±0.003	0.297 ±0.002	0.318 ±0.004
Pu239		0.164 ±0.002	0.156 ±0.002	0.147 ±0.001	0.127 ±0.001	0.0917 ±0.0011

See Pu Report.

APPENDIX 16

18–GROUP CROSS SECTIONS

(a) 18–Group Cross Sections used in CRAM Calculations

BeO

Group	σ_{tr}	σ_{rem}	$\sigma_{g\to g-3}$	$\sigma_{g\to g-2}$	$\sigma_{g\to g-1}$	$\sigma_{g\to g+1}$	$\sigma_{g\to g+2}$	$\sigma_{g\to g+3}$	$\sigma_{g\to g+4}$
1	2.172	1.324	–	–	–	1.242	0.35	0.0	0.0
2	2.455	0.732	–	–	0.0	0.7	0.12	0.0	0.0
3	5.61	2.109	–	0.0	0.0	2.109	0.0	0.0	0.0
4	6.94	1.815	0.0	0.0	0.0	1.815	0.0	0.0	0.0
5	7.65	0.971	0.0	0.0	0.0	0.971	0.0	0.0	0.0
6	8.44	0.881	0.0	0.0	0.0	0.881	0.0	0.0	0.0
7	8.83	0.935	0.0	0.0	0.0	0.935	0.0	0.0	0.0
8	9.01	1.06	0.0	0.0	0.0	1.06	0.0	0.0	0.0
9	9.06	1.06	0.0	0.0	0.0	1.06	0.0	0.0	0.0
10	9.10	1.68	0.0	0.0	0.0	1.68	0.0	0.0	0.0
11	9.10	1.6803	0.0	0.0	0.0	1.68	0.0	0.0	0.0
12	9.10	1.6804	0.0	0.0	0.0	1.68	0.0	0.0	0.0
13	9.10	1.6807	0.0	0.0	0.0	1.68	0.0	0.0	0.0
14	9.10	1.4985	0.0	0.0	0.0	1.4795	0.0171	0.0006	0.0001
15	9.10	1.1342	0.0	0.0	0.0581	1.013	0.0527	0.0085	–
16	9.10	0.604	0.0	0.0	0.1567	0.3298	0.1123	–	–
17	9.00	0.3951	0.0	0.0065	0.2869	0.0933	–	–	–
18	8.306	0.3126	0.0014	0.1614	0.1406	–	–	–	–

Aluminium

Group	σ_{tr}	σ_{rem}	$\sigma_{g\to g+1}$	$\sigma_{g\to g+2}$	$\sigma_{g\to g+3}$
1	1.929	0.808	0.642	0.120	0.030
2	2.322	0.634	0.380	0.220	0.034
3	2.344	0.578	0.395	0.170	0.012
4	2.896	0.264	0.264	0.0	0.0
5	3.519	0.188	0.188	0.0	0.0
6	2.921	0.123	0.123	0.0	0.0
7	1.458	0.06	0.06	0.0	0.0
8	1.410	0.05	0.05	0.0	0.0
9	1.410	0.05	0.05	0.0	0.0
10	1.460	0.10	0.10	0.0	0.0
11	1.470	0.11	0.10	0.0	0.0
12	1.490	0.12	0.10	0.0	0.0
13	1.510	0.13	0.10	0.0	0.0
14	1.550	0.14	0.10	0.0	0.0
15	1.550	0.17	0.10	0.0	0.0
16	1.570	0.21	0.10	0.0	–
17	1.640	0.28	0.10	–	–
18	1.540	0.18	–	–	–

(continued)

APPENDIX 16 (continued)

Oxygen

Group	σ_{tr}	σ_{rem}	$\sigma_{g\rightarrow g+1}$
1	1.33	0.464	0.421
2	1.18	0.191	0.191
3	3.23	0.902	0.902
4	3.63	0.556	0.556
5	3.71	0.337	0.337
6	3.26	0.231	0.231
7	3.55	0.255	0.255
8	3.64	0.23	0.23
9	3.64	0.23	0.23
10	3.64	0.46	0.46
11	3.64	0.46	0.46
12	3.64	0.46	0.46
13	3.64	0.46	0.46
14	3.64	0.46	0.46
15	3.64	0.46	0.46
16	3.64	0.46	0.46
17	3.64	0.46	0.46
18	3.6412	0.0002	–

Th 232 σ_p = 2000 barns

Group	σ_{tr}	σ_{rem}	$\nu\sigma_f$	$\sigma_{g\rightarrow g+1}$	$\sigma_{g\rightarrow g+2}$	$\sigma_{g\rightarrow g+3}$	$\sigma_{g\rightarrow g+4}$	$\sigma_{g\rightarrow g+5}$
1	✓ 4.00	2.36	0.384	0.33	0.46	0.79	0.53	0.07
2	✓ 4.22	2.19	0.230	0.35	0.96	0.64	0.09	0.0
3	✓ 4.32	1.53	0.021	0.80	0.55	0.10	0.0	0.0
4	✓ 5.04	0.71	0.0	0.50	0.08	0.0	0.0	0.0
5	✓ 7.87	0.29	0.0	0.08	0.0	0.0	0.0	0.0
6	✓ 13.48	0.54	0.0	0.06	0.0	0.0	0.0	0.0
7	✓ 14.5	0.67	0.0	0.07	0.0	0.0	0.0	0.0
8	14.5	1.9	0.0	0.07	0.0	0.0	0.0	0.0
9	20.84	8.91	0.0	0.07	0.0	0.0	0.0	0.0
10	28.16	16.23	0.0	0.07	0.0	0.0	0.0	0.0
11	22.04	10.11	0.0	0.07	0.0	0.0	0.0	0.0
12	✓ 12.5	0.57	0.0	0.07	0.0	0.0	0.0	0.0
13	12.26	0.33	0.0	0.07	0.0	0.0	0.0	0.0
14	12.84	0.91	0.0	0.07	0.0	0.0	0.0	–
15	14.4	2.5	0.0	0.07	0.0	0.0	–	–
16	16.0	4.08	0.0	0.07	0.0	–	–	–
17	18.0	6.07	0.0	0.07	–	–	–	–
18	19.6	7.60	0.0	–	–	–	–	–

(continued)

APPENDIX 16 (continued)

U238 σ_p = 2000 barns

Group	σ_{tr}	σ_{rem}	$\nu\sigma_f$	$\sigma_{g\to g+1}$	$\sigma_{g\to g+2}$	$\sigma_{g\to g+3}$	$\sigma_{g\to g+4}$	$\sigma_{g\to g+5}$
1	4.0	2.746	2.037	0.33	0.46	0.79	0.53	0.07
2	4.4	2.575	1.297	0.35	0.96	0.64	0.09	0.0
3	4.5	1.594	0.111	0.80	0.55	0.10	0.0	0.0
4	5.25	0.72	0.0	0.50	0.08	0.0	0.0	0.0
5	8.2	0.24	0.0	0.08	0.0	0.0	0.0	0.0
6	12.0	0.55	0.0	0.10	0.0	0.0	0.0	0.0
7	14.0	0.75	0.0	0.05	0.0	0.0	0.0	0.0
8	15.0	2.05	0.0	0.05	0.0	0.0	0.0	0.0
9	18.91	8.975	0.0	0.05	0.0	0.0	0.0	0.0
10	22.55	12.6	0.0	0.05	0.0	0.0	0.0	0.0
11	31.40	21.45	0.0	0.05	0.0	0.0	0.0	0.0
12	58.86	48.91	0.0	0.05	0.0	0.0	0.0	0.0
13	10.50	0.552	0.0	0.05	0.0	0.0	0.0	0.0
14	10.63	0.675	0.0	0.05	0.0	0.0	0.0	–
15	10.87	0.925	0.0	0.05	0.0	0.0	–	–
16	11.43	1.48	0.0	0.05	0.0	–	–	–
17	12.23	2.28	0.0	0.05	–	–	–	–
18	12.4	2.40	0.0	–	–	–	–	–

U238 σ_p = 400 barns

Group	σ_{tr}	σ_{rem}	$\nu\sigma_f$	$\sigma_{g\to g+1}$	$\sigma_{g\to g+2}$	$\sigma_{g\to g+3}$	$\sigma_{g\to g+4}$	$\sigma_{g\to g+5}$
9	14.5	4.57	0.0	0.05	0.0	0.0	0.0	0.0
10	18.10	8.10	0.0	0.05	0.0	0.0	0.0	0.0
11	20.78	10.33	0.0	0.05	0.0	0.0	0.0	0.0
12	30.62	20.67	0.0	0.05	0.0	0.0	0.0	0.0

(continued)

U235 σ_p = 100 barns

Group	σ_{tr}	σ_{rem}	$\nu\sigma_f$	$\sigma_{g\to g+1}$	$\sigma_{g\to g+2}$	$\sigma_{g\to g+3}$	$\sigma_{g\to g+4}$	$\sigma_{g\to g+5}$
1	4.25	3.05	4.08	0.27	0.37	0.65	0.44	0.06
2	4.50	2.73	3.254	0.24	0.67	0.45	0.07	0.0
3	4.65	2.35	3.093	0.55	0.40	0.07	0.0	0.0
4	5.20	1.78	2.977	0.35	0.08	0.0	0.0	0.0
5	7.90	1.74	3.492	0.08	0.0	0.0	0.0	0.0
6	12.4	3.20	6.023	0.05	0.0	0.0	0.0	0.0
7	15.1	5.55	10.23	0.05	0.0	0.0	0.0	0.0
8	21.1	11.15	19.24	0.05	0.0	0.0	0.0	0.0
9	35.5	25.55	42.57	0.05	0.0	0.0	0.0	0.0
10	62.8	52.85	83.89	0.05	0.0	0.0	0.0	0.0
11	59.89	49.94	66.96	0.05	0.0	0.0	0.0	0.0
12	39.77	29.82	40.62	0.05	0.0	0.0	0.0	0.0
13	37.88	27.93	52.16	0.05	0.0	0.0	0.0	0.0
14	80.03	70.08	144.9	0.05	0.0	0.0	0.0	–
15	214.4	204.45	403.4	0.05	0.0	0.0	–	–
16	323.6	313.6	647.1	0.05	0.0	–	–	–
17	571.3	571.3	1146.0	0.05	–	–	–	–
18	614.0	604.0	1231.0	–	–	–	–	–

(b) 18-Group Fission Cross Sections used in Fission Ratio Calculations

Group	U233	U235	Pu239
1	1.75	1.21	1.90
2	1.83	1.22	1.95
3	1.89	1.22	1.83
4	1.94	1.20	1.70
5	2.24	1.43	1.67
6	3.23	2.50	2.04
7	5.98	4.22	3.04
8	8.96	7.95	4.06
9	23.9	17.59	15.2
10	53.0	60.05	10.1
11	101.6	58.47	88.1
12	89.6	24.3	33.5
13	288.8	24.8	21.9
14	131.5	61.9	147.0
15	182.5	166.7	1576.0
16	293.2	267.4	496.8
17	457.0	473.4	608.0
18	447.0	508.7	655.0

$\sigma_p = \infty$

APPENDIX 17

ENERGY SPECTRUM AT CENTRE OF CRITICAL SPHERE

(a) BeO/Fertile Mixture/U235 Assemblies

Group	Lethargy Range (from 10 MeV)	Normalised Flux at Centre of Critical Sphere							
		Lattice U I	Lattice U II	Lattice U III	Lattice U IV	Lattice Th I	Lattice Th II	Lattice Th III	Lattice Th IV
1	1.204	910	804	632	536	887	776	577	475
2	1.966	5832	5233	4207	3632	5753	5117	3956	3317
3	2.408	6814	6046	4770	4076	6674	5860	4422	3655
4	3.219	6201	5499	4335	3703	6072	5328	4018	3320
5	4.605	7580	6752	5364	4603	7447	6565	5004	4160
6	6.377	6804	6093	4893	4220	6702	5952	4596	3852
7	8.0	7015	6317	5123	4450	6931	6200	4856	4103
8	10.0	4884	4430	3633	3174	4847	4371	3472	2957
9	12.0	4610	4224	3513	3091	4508	4109	3320	2852
10	13.0	5444	5041	4244	3756	5223	4810	3944	3412
11	14.0	5080	4742	4045	3600	4885	4545	3781	3294
12	15.0	4640	4366	3758	3362	4712	4422	3727	3269
13	16.0	4471	4236	3684	3311	4557	4310	3677	3245
14	17.0	4961	4788	4276	3898	5075	4860	4307	3864
15	18.0	6732	7088	7287	7229	6931	7307	7508	7413
16	19.0	9859	12206	16021	18057	10238	12703	16979	19244
17	19.8	6000	8744	14159	17481	6287	9180	15300	19046
18	Thermal	2165	3388	6057	7819	2265	3547	6541	8522

(continued)

APPENDIX 17 (continued)

(b) BeO/U235 Assemblies

Group	Lethargy Range (from 10 MeV)	Normalised Flux at Centre of Critical Sphere			
		U5 1	U5 2	U5 3	U5 4
1	1.204	942	744	550	442
2	1.966	5966	4836	3665	2999
3	2.408	6957	5529	4085	3302
4	3.219	6238	4947	3641	2941
5	4.605	7519	6009	4452	3613
6	6.377	6649	5363	4006	3271
7	8.0	6758	5506	4149	3411
8	10.0	4685	3862	2940	2430
9	12.0	4452	3731	2879	2397
10	13.0	5330	4543	3548	2971
11	14.0	5065	4386	3466	2919
12	15.0	4838	4246	3391	2870
13	16.0	4634	4116	3318	2823
14	17.0	5110	4688	3889	3365
15	18.0	6876	7386	7304	7075
16	19.0	9962	14308	18656	20898
17	19.8	5926	11321	18211	22275
18	Thermal	2090	4476	7848	9993

APPENDIX 18

DISTANCES OF MEASURING POSITIONS FROM THE REFERENCE FACES

E – W Position N – S Position	Distance From E. Face (cm) Distance From N. Face (cm)
4	10.16
5	12.70
6	15.24
7	17.78
8	20.32
9	22.86
10	25.40
11	27.94
12	30.48
13	33.02
14	35.56
15	38.10
16	40.64
17	43.18
18	45.72
19	48.26
20	50.80

Vertical Position	Distance From Bottom Face
2	71.88
3	69.08
4	66.28
5	63.48
6	60.69
7	57.89
8	55.09
9	52.29
10	49.49
11	46.69
12	43.89
13	41.09
14	38.29

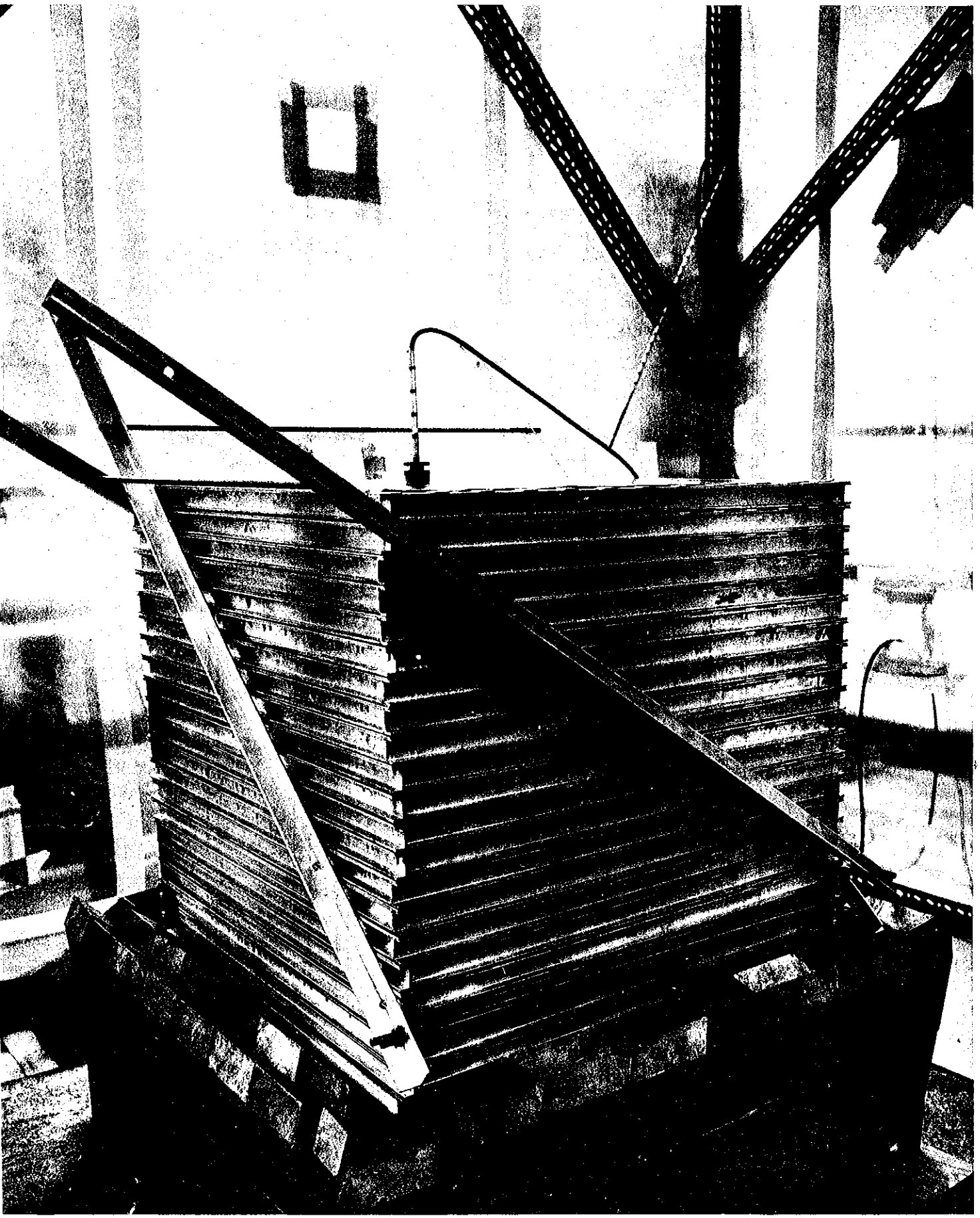

FIGURE 1 GENERAL VIEW OF STACK

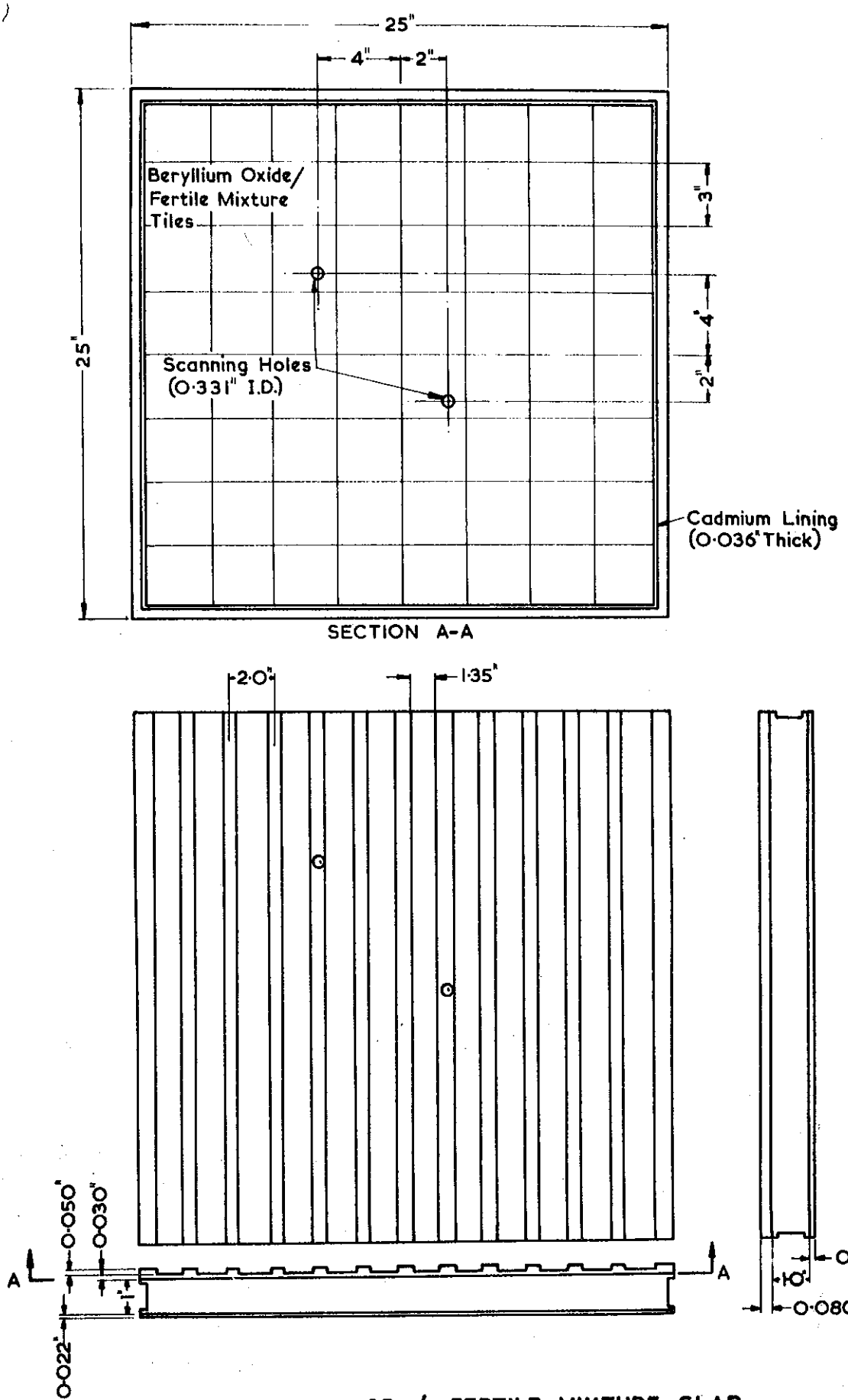

FIGURE 2 CANNED MODERATOR / FERTILE MIXTURE SLAB

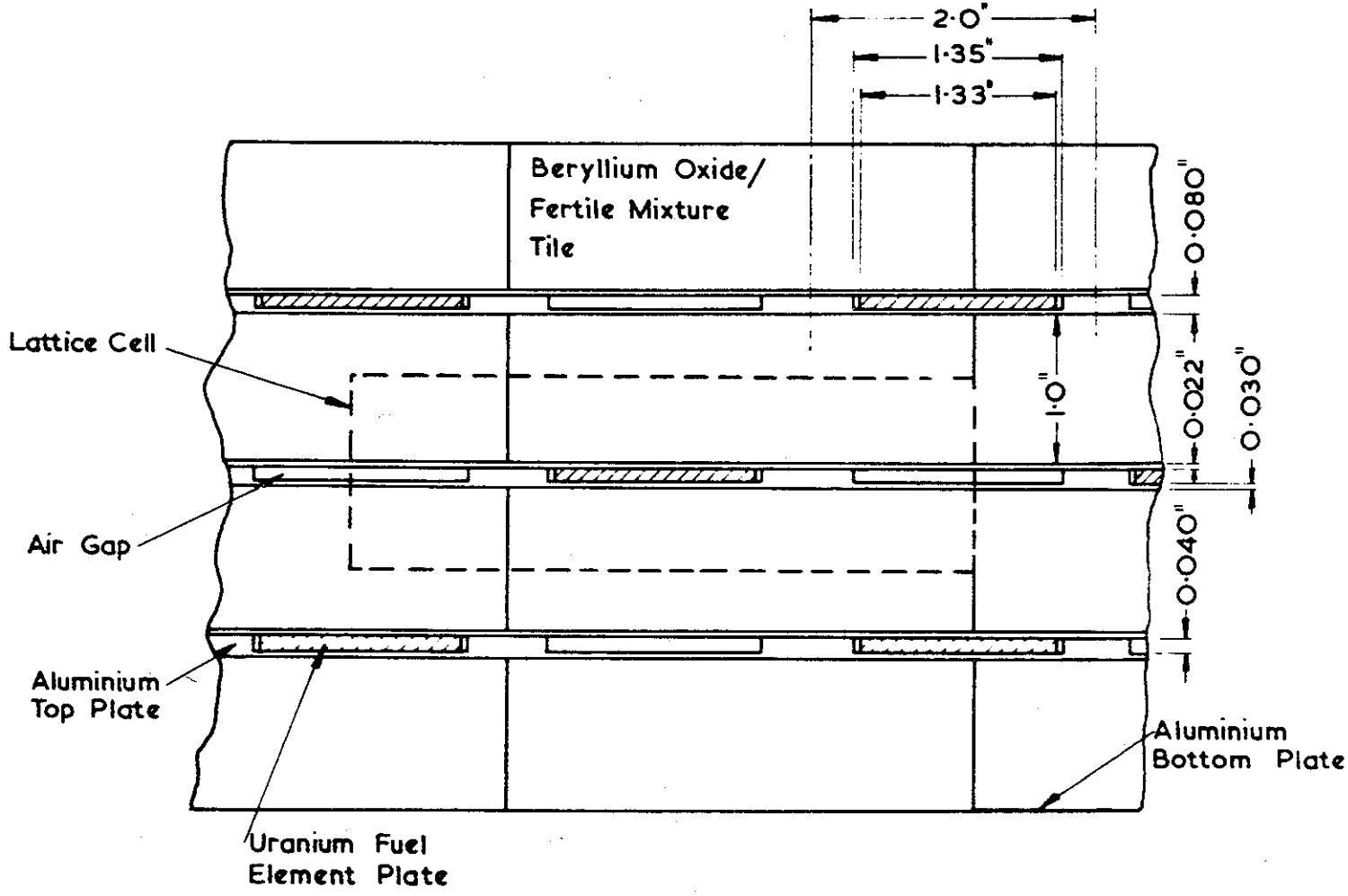

FIGURE 3 LATTICE IA — REPRESENTATIVE SECTION OF EAST FACE

P837

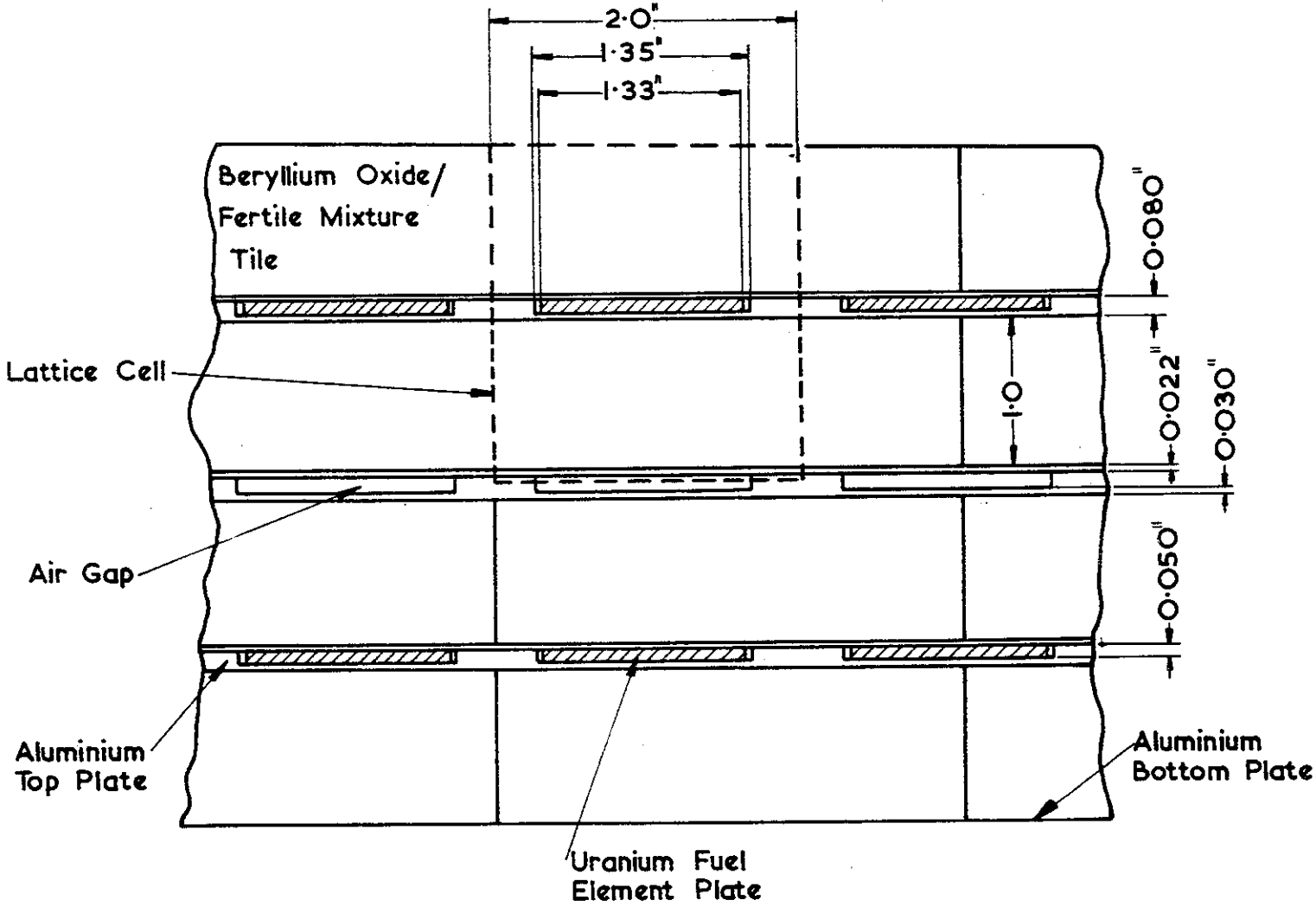

FIGURE 4 LATTICE IB—REPRESENTATIVE SECTION OF EAST FACE

P837

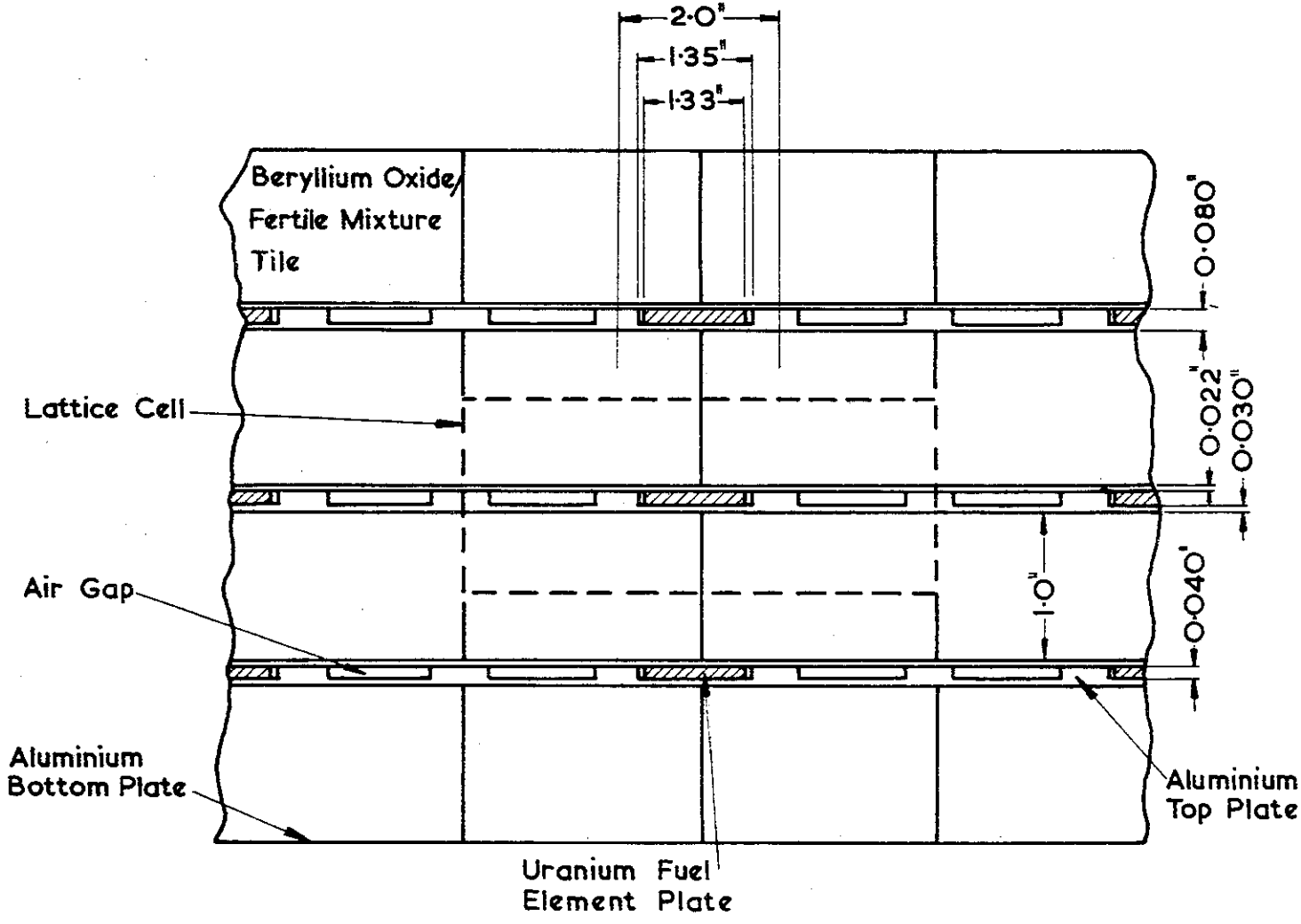

FIGURE 5 LATTICE II — REPRESENTATIVE SECTION OF EAST FACE

P837

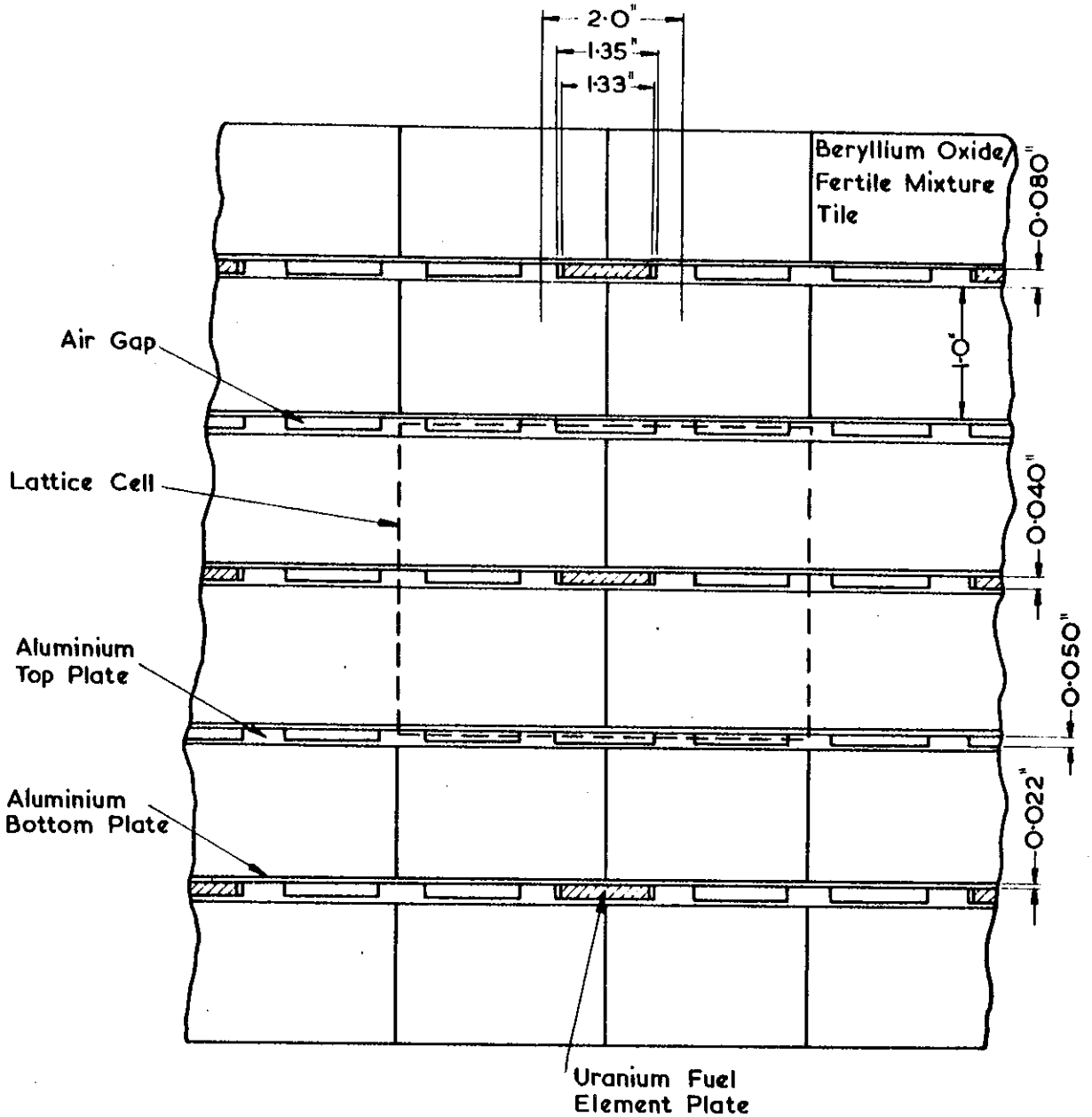

FIGURE 6 LATTICE III—REPRESENTATIVE SECTION OF EAST FACE

P837

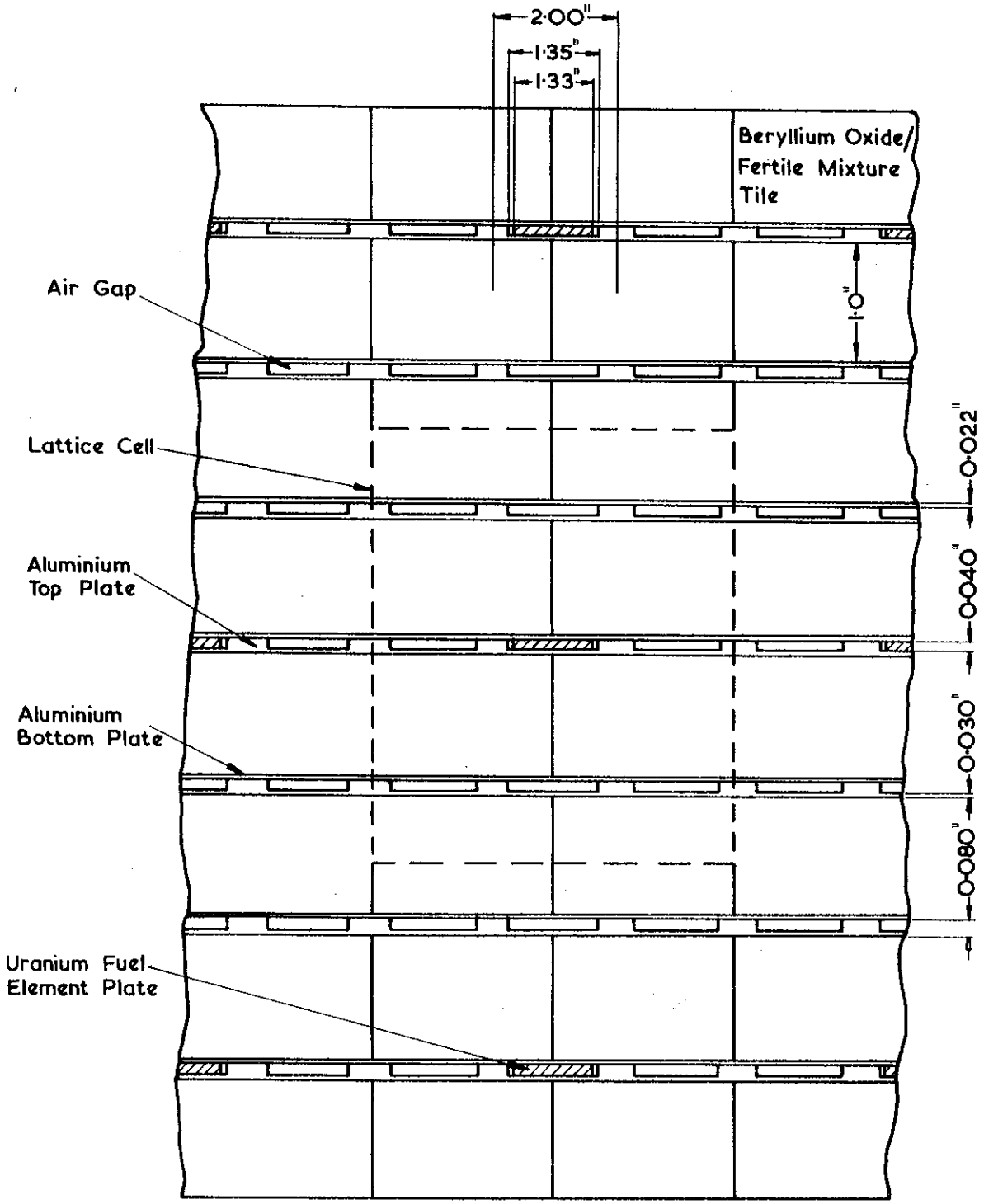

FIGURE 7 LATTICE IV — REPRESENTATIVE SECTION OF EAST FACE

P837

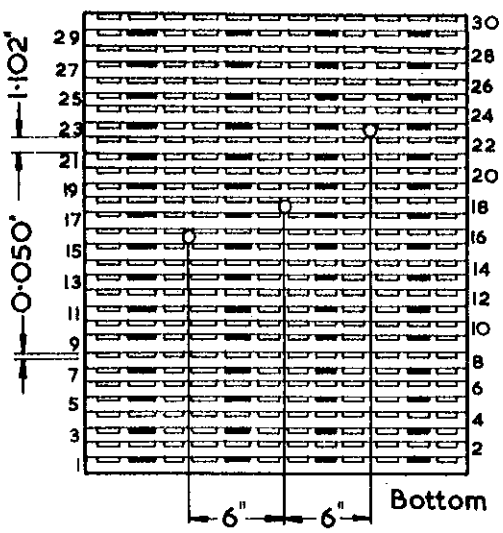

EAST FACE

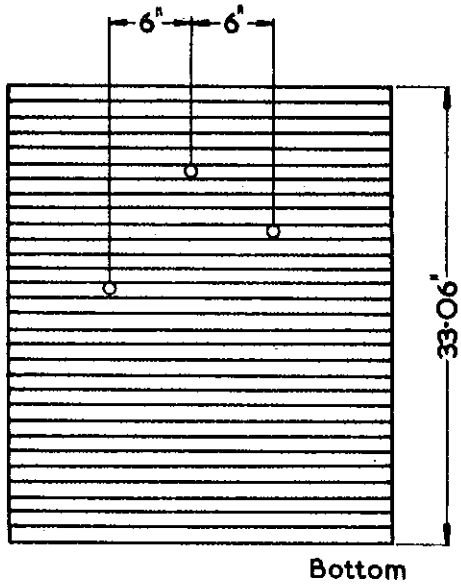

SOUTH FACE

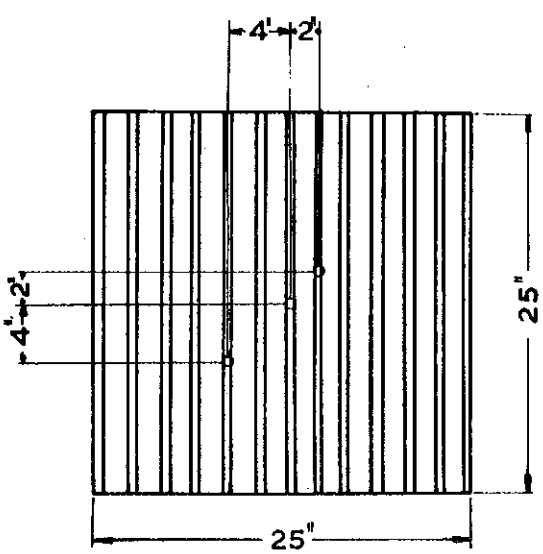

TOP FACE

FIGURE 8 SCANNING HOLE POSITIONS IN TYPICAL STACK (LATTICE II)

P837

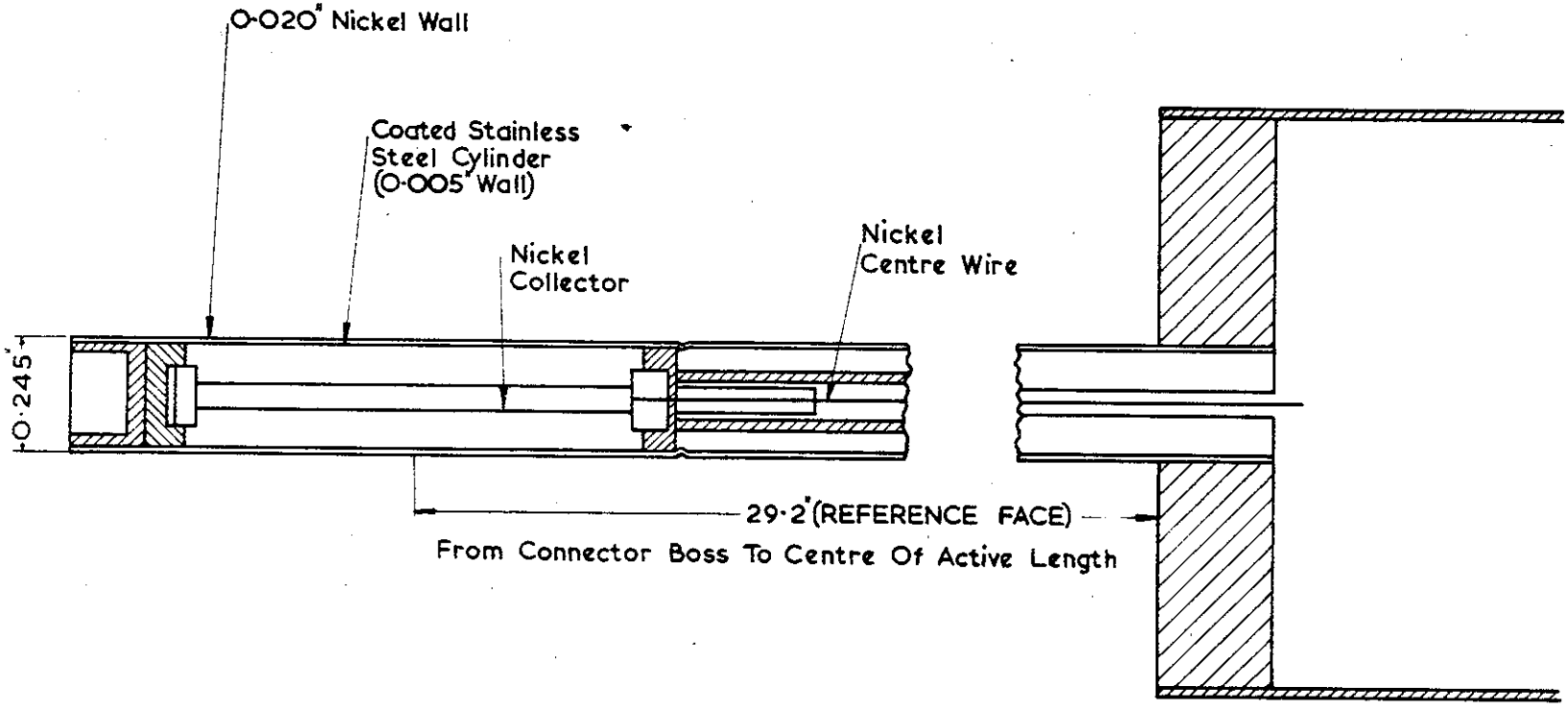

FIGURE 9A RIGID STEM FISSION CHAMBER

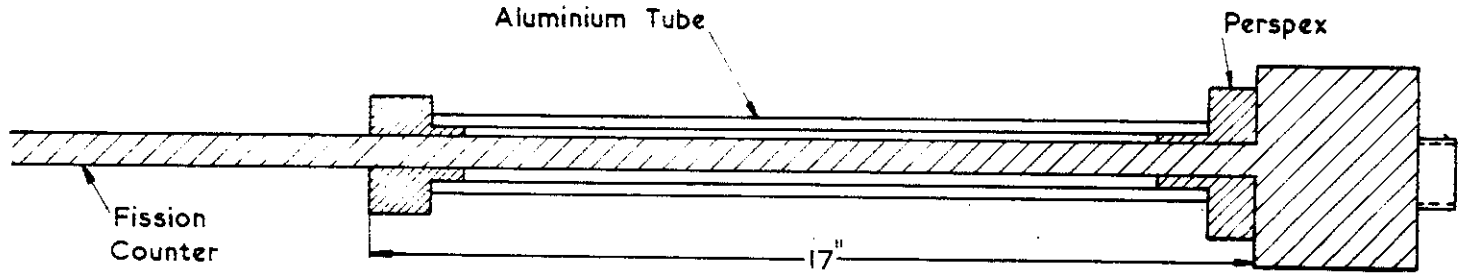

FIGURE 9B SPACER

P837

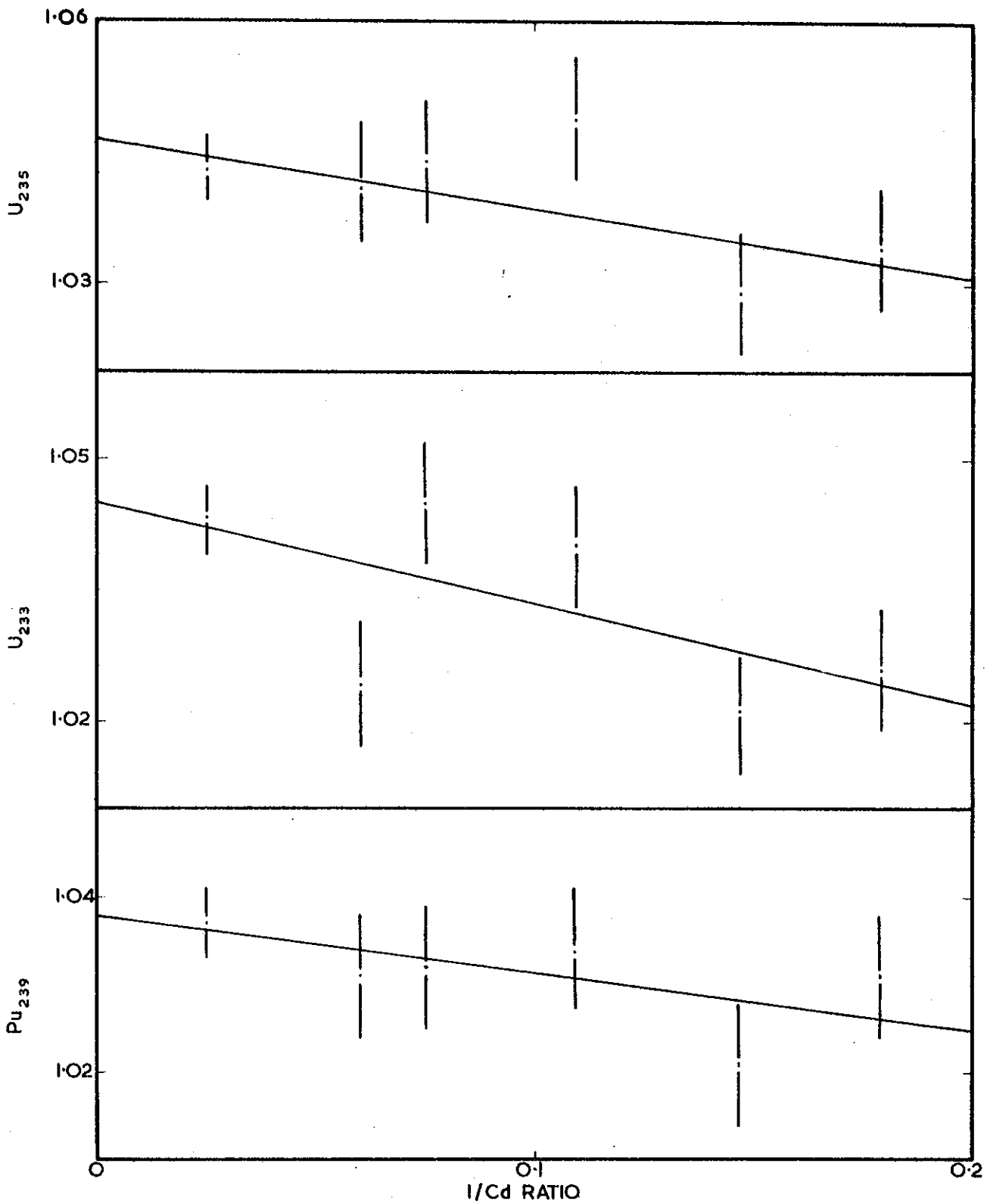

FIGURE 10 FLUX DEPRESSION BY NICKEL WALLS

P 8 37

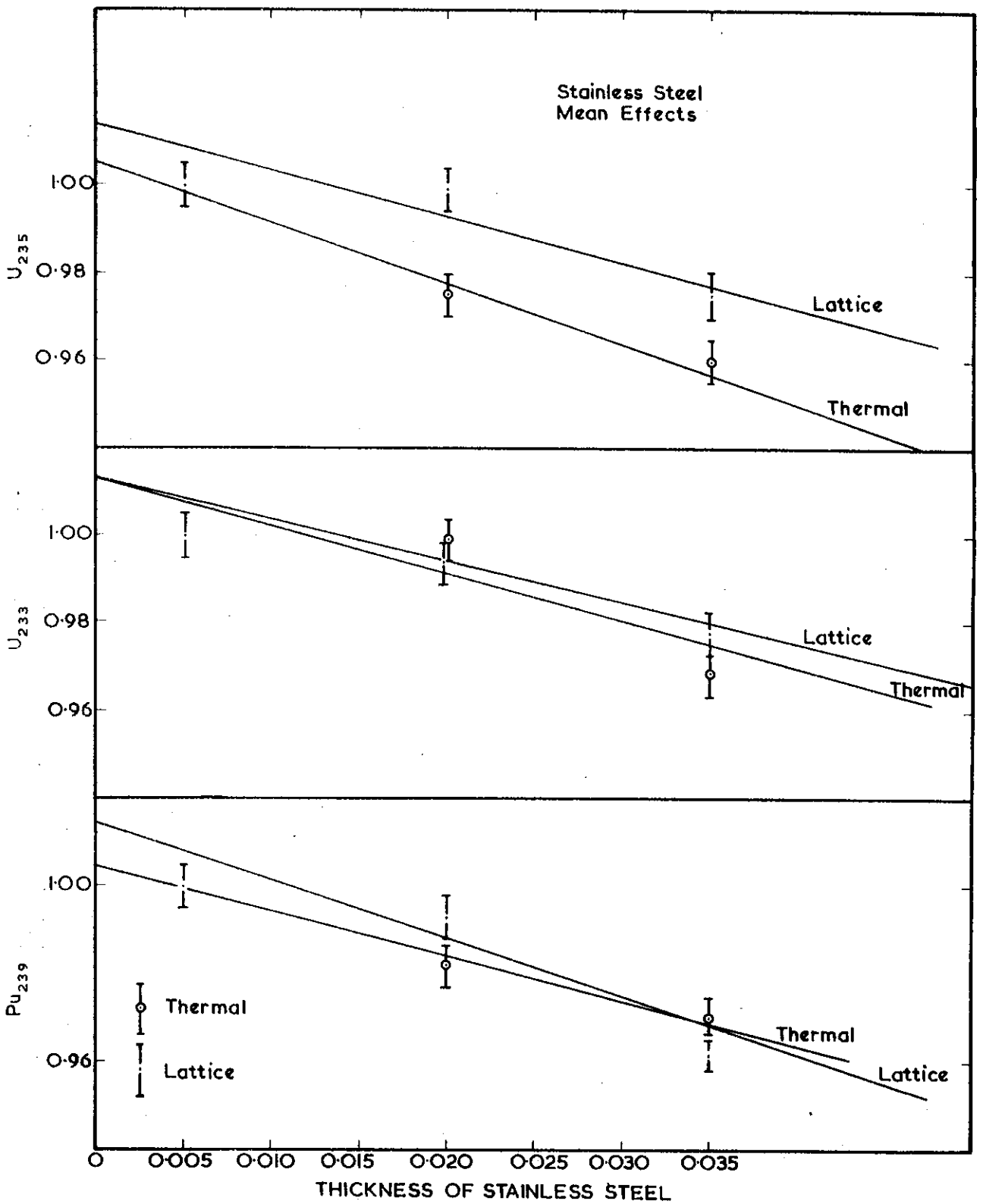

FIGURE II FLUX DEPRESSION BY STAINLESS STEEL

P837

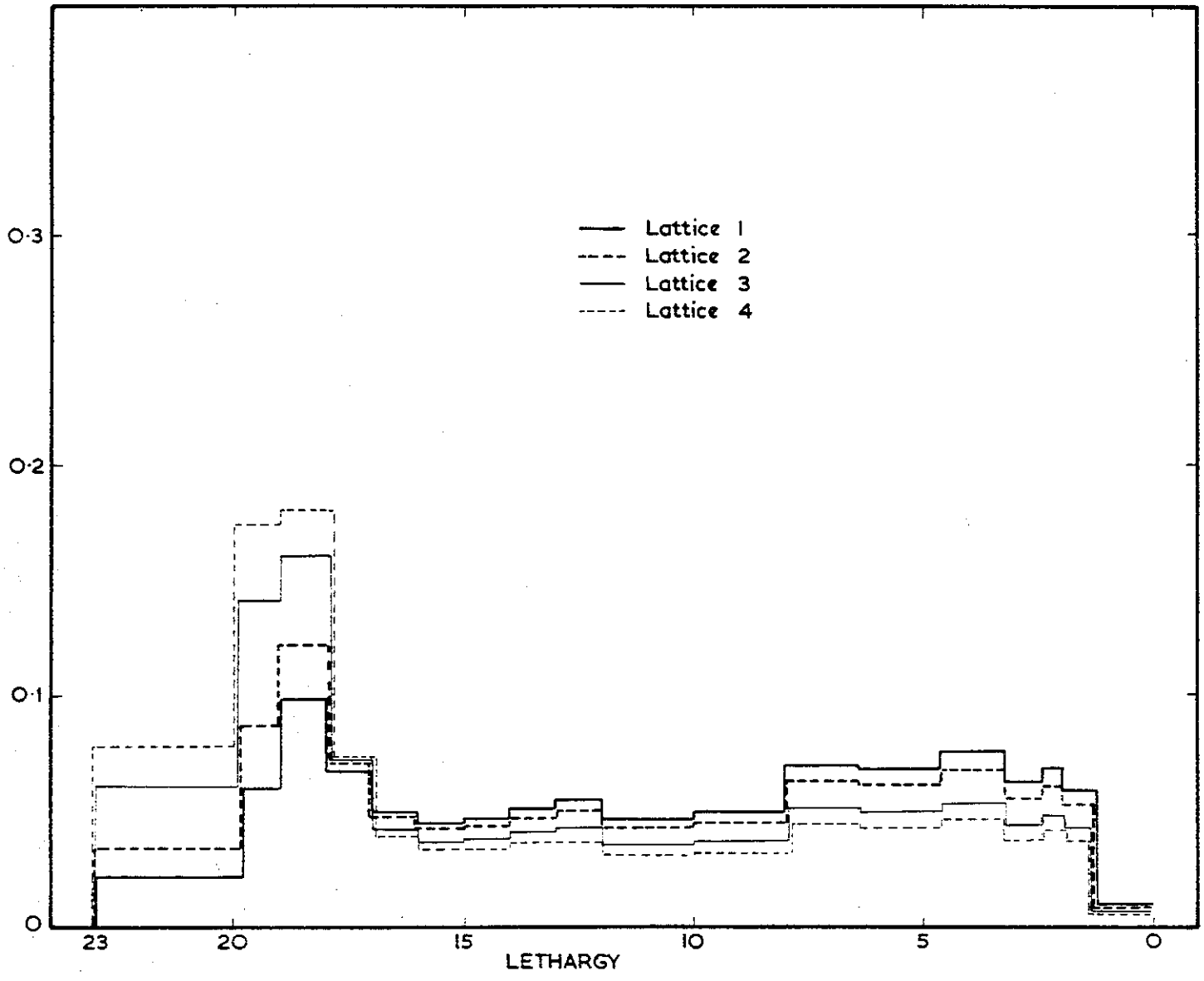

FIGURE 12 NORMALISED NEUTRON FLUX / UNIT LETHARGY, BeO / UO_2 ASSEMBLIES

P637

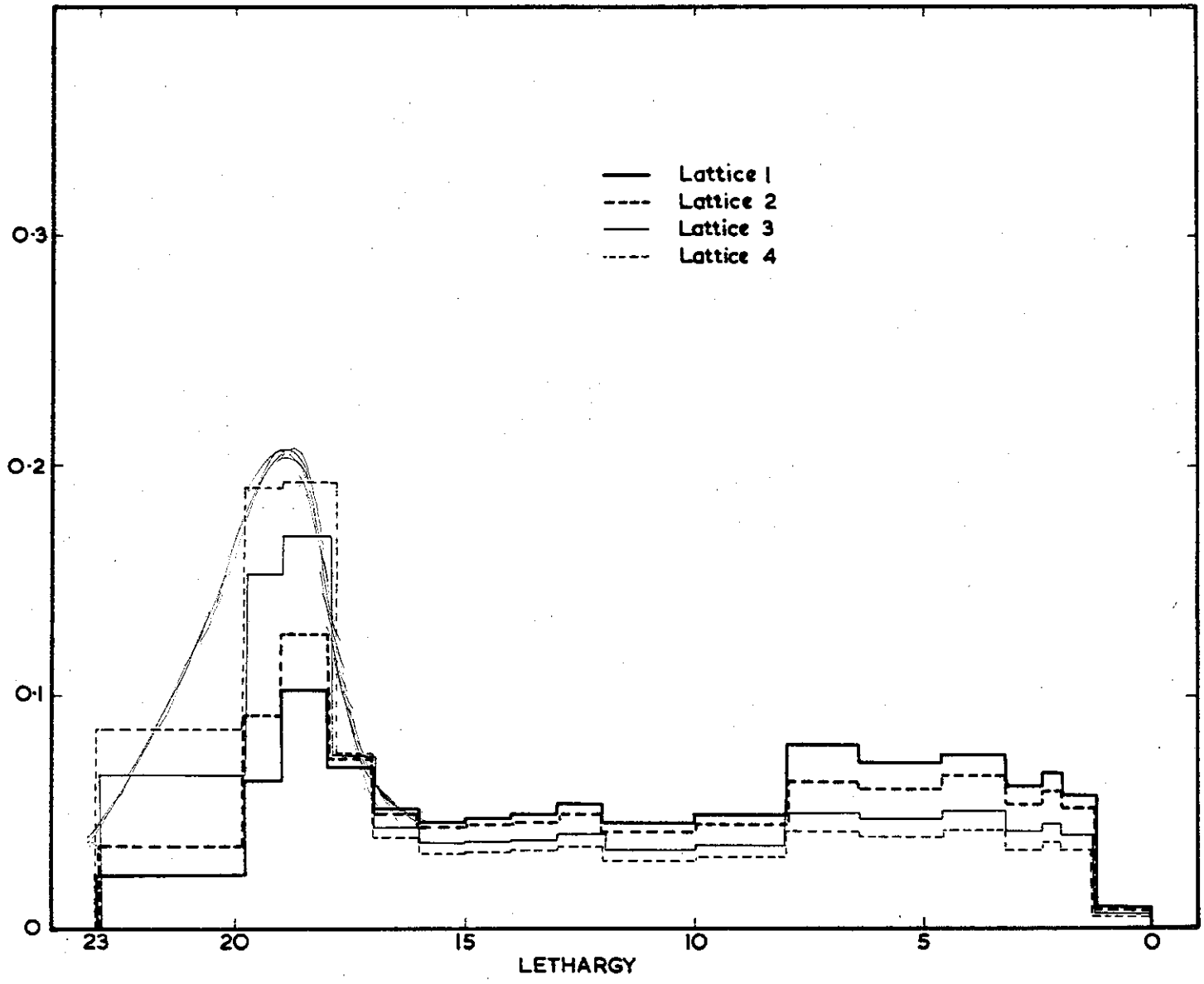

FIGURE 13 NORMALISED NEUTRON FLUX / UNIT LETHARGY, BeO/ThO_2 ASSEMBLIES

P837

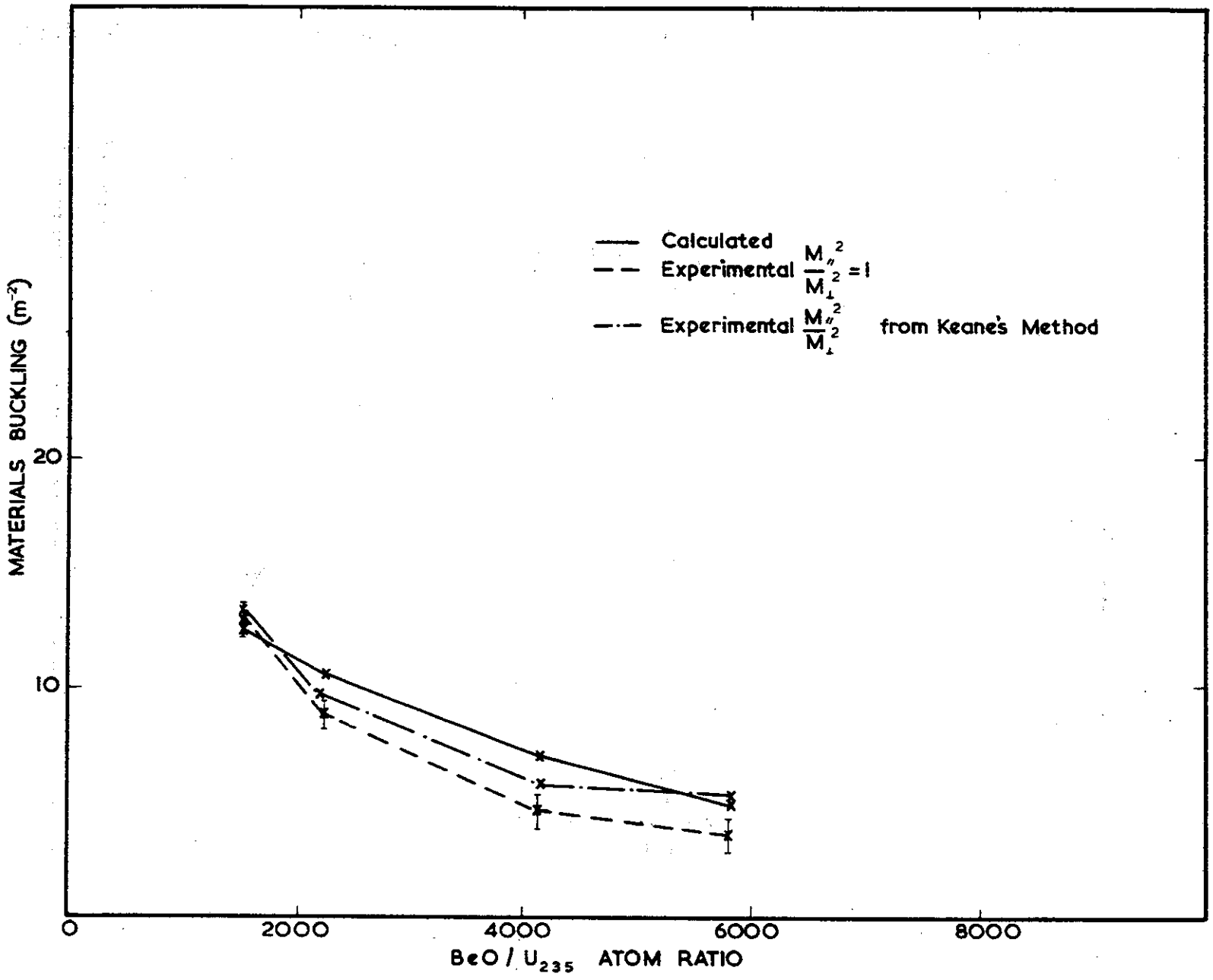

FIGURE 14 MATERIALS BUCKLING BeO / UO_2 ASSEMBLIES

P837

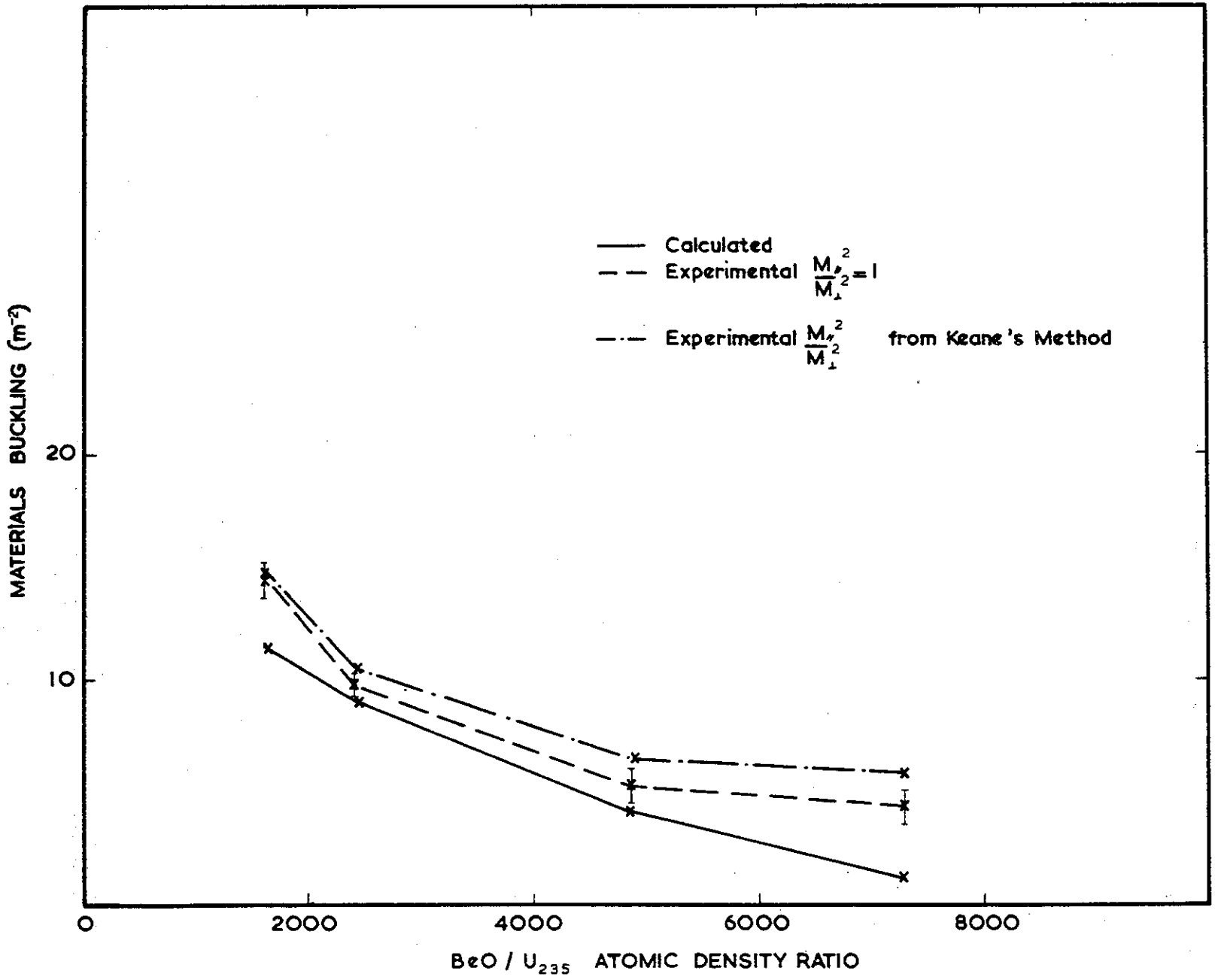

FIGURE 15 MATERIALS BUCKLING BeO / ThO_2 ASSEMBLIES

P837

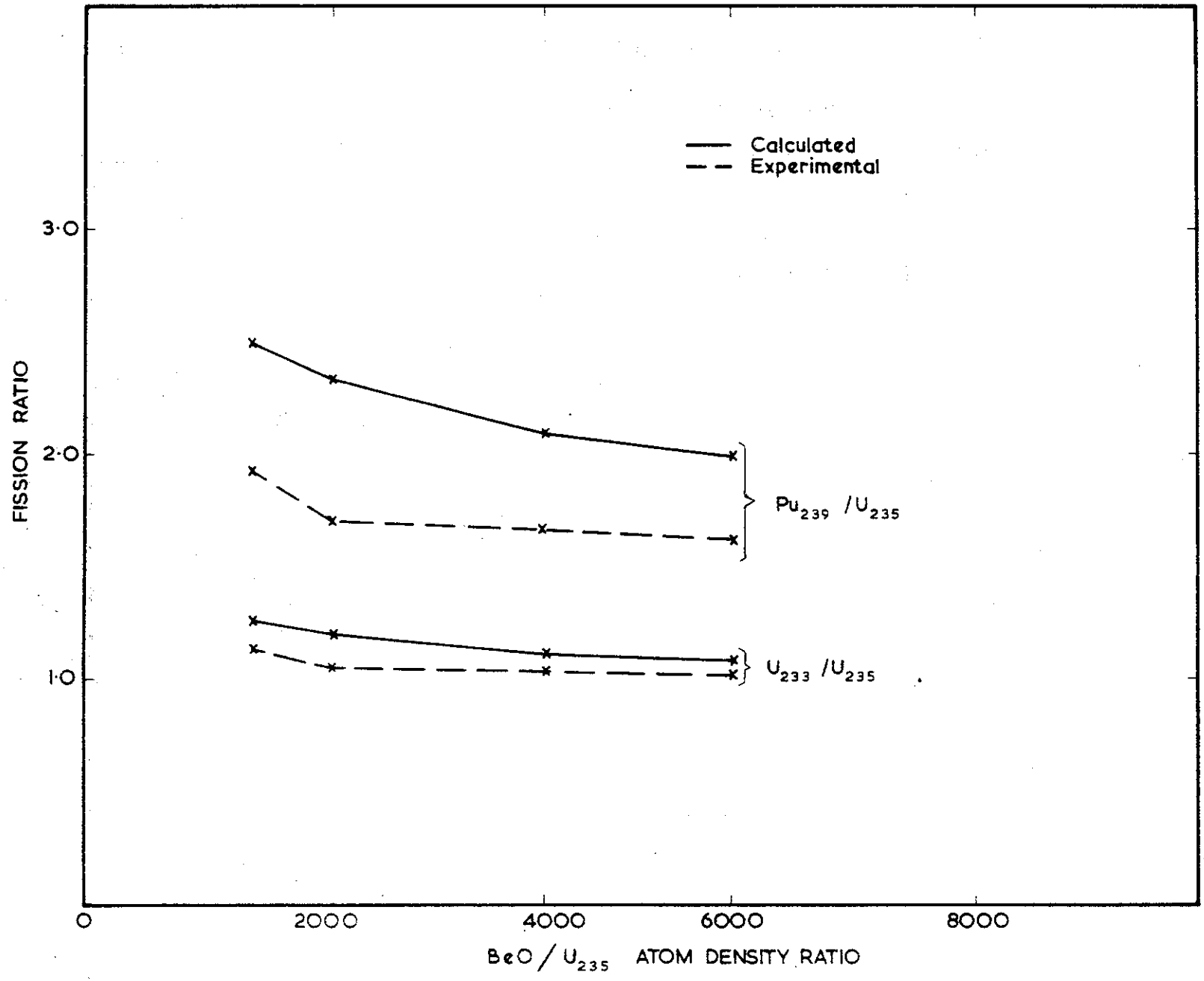

FIGURE 16 FISSION RATIOS, BeO / UO_2 ASSEMBLIES

P837

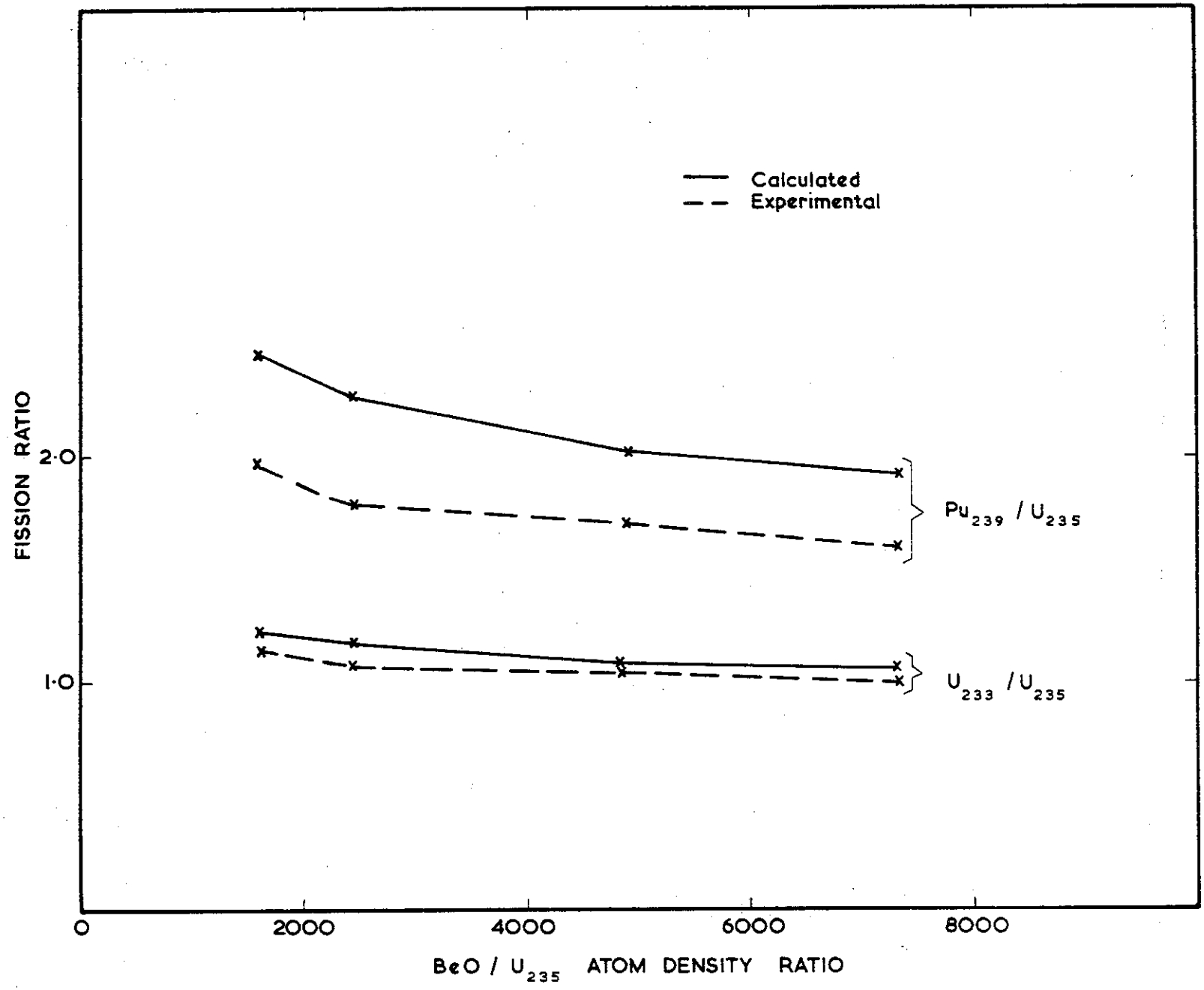

FIGURE 17 FISSION RATIO, BeO / ThO_2 ASSEMBLIES

P837

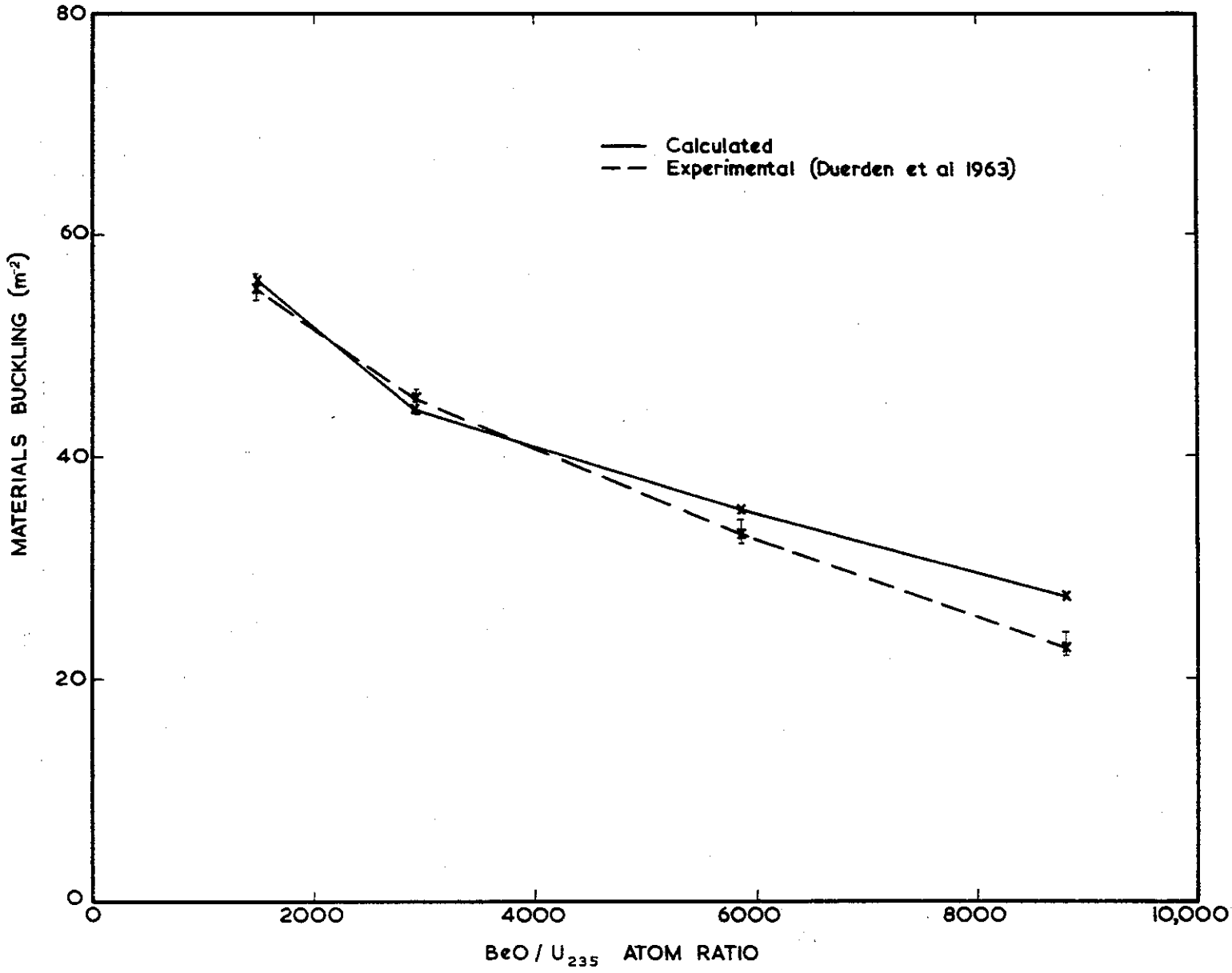

FIGURE 18 MATERIALS BUCKLING BeO/ U_{235} ASSEMBLIES

P837

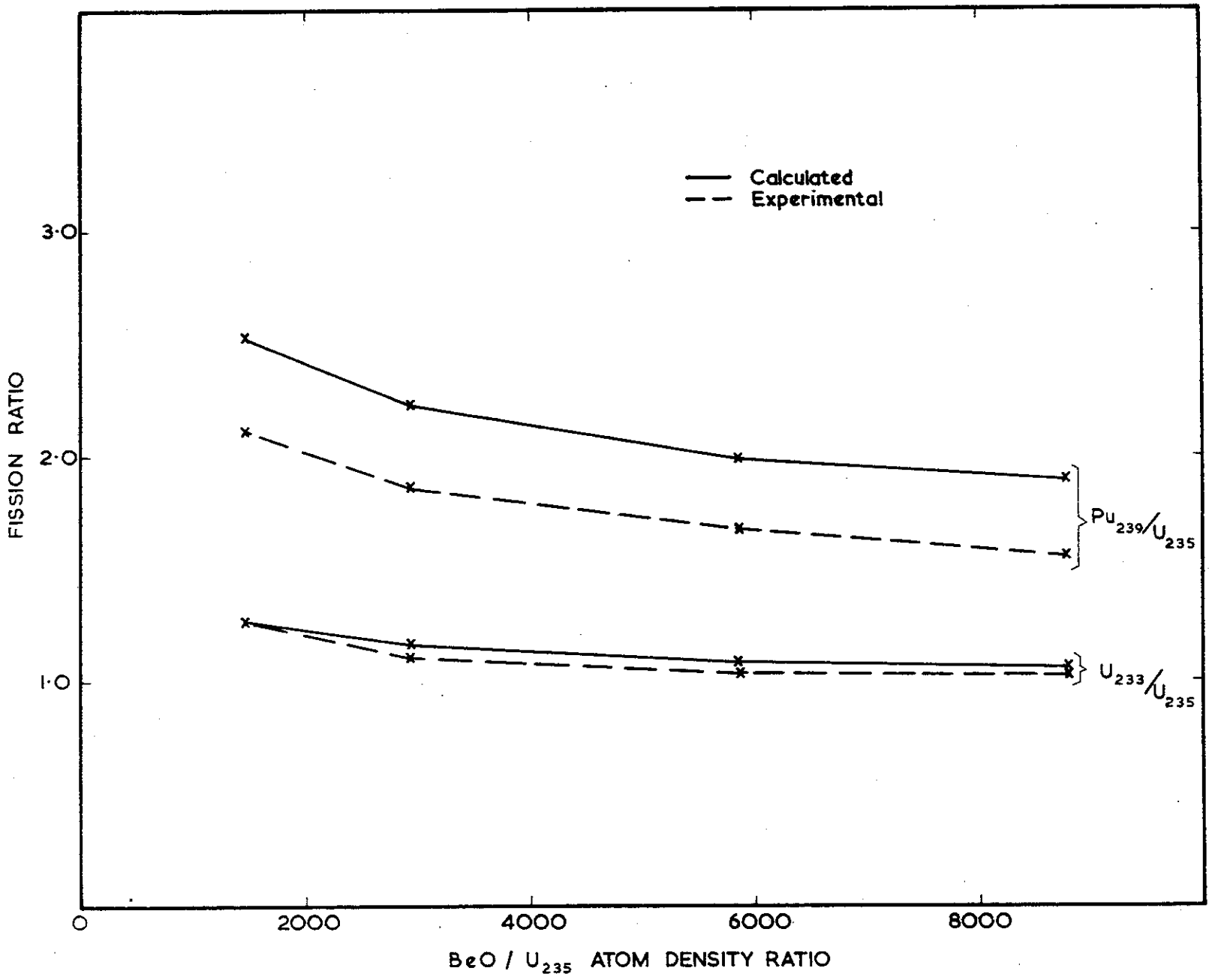

FIGURE 19 FISSION RATIO, BeO / U_{235} ASSEMBLIES

P837